scientific reports

Check for updates

OPEN

Development of a new hydraulic electric index for rock typing in carbonate reservoirs

Milad Mohammadi[1], Mohammad Emami Niri[2]✉, Abbas Bahroudi[1], Aboozar Soleymanzadeh[3] & Shahin Kord[3]

Rock typing techniques have relied on either electrical or hydraulic properties. The study introduces a novel approach for reservoir rock typing, the hydraulic-electric index (HEI), which combines the strengths of traditional electrical and hydraulic rock typing methods to characterize carbonate reservoirs more accurately. By normalizing the ratio of permeability and formation resistivity factor (K/FRF) with respect to porosity, the HEI method is applied to two datasets of carbonate core samples: dataset 1 consists of 112 carbonate core samples from the Tensleep formation in the Bighorn basin of Wyoming and Montana, and dataset 2 includes 81 carbonate core samples from the Asmari formation in the south-west of Iran. Statistical analysis confirms the effectiveness of the HEI in predicting permeability, with high determination coefficients for both datasets (resulting in determination coefficients (R^2) of 0.965 and 0.904 for dataset 1 and dataset 2, respectively). The results classify the rock samples into distinct rock types, nine rock types for dataset 1 and four rock types for dataset 2, and demonstrate the HEI ability to capture the relationship between hydraulic conductivity and electrical resistivity in carbonate reservoir rocks. Applying the HEI method to the validation dataset yielded highly accurate permeability predictions, with average of determination coefficients of 0.883 and 0.859 for dataset 1 and dataset 2, respectively. Validation of the HEI method further confirms (20% of the dataset was set aside for validation, while the remaining 80% was used for the rock typing approach (5 folds)) its accuracy in predicting permeability, highlighting its robust predictive capacity for estimating permeability in carbonate reservoirs.

Keywords Hydraulic-electric index (HEI), Rock typing, Iranian carbonate reservoir, Permeability, Reservoir characterization

List of symbols

a	Tortuosity factor
K	Permeability (mD)
m	Cementation factor
ϕ	Porosity
CZI	Current zone indicator
ERI	Electrical radius indicator
EQI	Electrical quality index
EZI	Electrical zone indicator
FZI	Flow zone indicator
FRF	Formation resistivity factor
HEI	Hydraulic-electric index
HFU	Hydraulic flow unit
EFU	Electrical flow unit
RQI	Rock quality index
MGEMTIP	Modified generalized effective medium theory of induced polarization

[1]School of Mining Engineering, College of Engineering, University of Tehran, Tehran, Iran. [2]Institute of Petroleum Engineering, School of Chemical Engineering, College of Engineering, University of Tehran, Tehran, Iran. [3]Department of Petroleum Engineering, Ahvaz Faculty of Petroleum, Petroleum University of Technology (PUT), Ahvaz, Iran. ✉email: Emami.m@ut.ac.ir

Subscript & superscript

R_w	Brine resistivity (ohm.m)
R_o	Brine-saturated rock resistivity (ohm.m)
R^2	Regression coefficient
σ_w	Brine conductivity (S/m)
σ_o	Rock conductivity (S/m)
ϕ_{HEI}	Hydraulic-electric index porosity
ϕ_N	Normalized porosity

Reservoir characterization is a critical endeavour in the geo-energy industry, playing an essential role in the efficient recovery of hydrocarbons and the optimization of reservoir management strategies[1–5]. Understanding the complex interplay between various rock properties is essential for predicting fluid flow behaviour and making informed decisions in exploration and production activities[6–9]. Carbonate reservoirs, in particular, suffer from unique challenges due to their complex pore systems and diagenetic alterations. As a result of these complexities, it is difficult to establish a general mathematical model or strategy that accurately predicts the critical petrophysical properties in carbonate reservoirs[10–14]. In addition, the conventional rock typing approaches may not fully capture the intricate nature of the carbonate rocks[15–17].

The significance of electrical rock typing lies in its ability to capture the electrical response of rocks, which is influenced by pore geometry, fluid saturation, mineralogy, and the presence of conductive minerals[18–21]. Electrical rock typing is a method of describing rocks in reservoirs based on their electrical properties. It involves the measurement of various electrical parameters, such as resistivity and classification of rocks into different electrical flow units (EFU)[22,23]. Electrical properties offer valuable insights into fluid distribution, connectivity, and flow behaviour within the subsurface. Otherwise, hydraulic rock typing focuses on permeability and porosity, which are influenced by factors like grain size, sorting, cementation, and diagenesis[24–26]. Understanding hydraulic rock types helps to predict fluid flow paths, identify flow barriers, and optimize reservoir development strategies[27–29]. These factors can vary significantly within a reservoir, leading to a complex relationship between permeability and porosity. Similarly, the FRF, which measures how easily electric currents can flow through a porous medium, is also affected by the complex pore structure of carbonate rocks[30]. The presence of different types of pores and their connectivity can significantly impact the FRF. In recent years, substantial advancements have been made in rock typing methodologies, driven by integrating advanced petrophysical measurements, data-driven analysis techniques, and machine-learning algorithms. These innovations have improved the accuracy and efficiency of rock typing, enabling more informed decision-making in oil and gas exploration and production[31–34].

The geometry of pores and interconnections between them significantly influences carbonate rock's electrical and hydraulic properties. This is especially noticeable for carbonate rock[35–38]. However, the relationship between permeability and FRF is not straightforward in carbonate reservoirs[39–41]. This is because carbonate rocks are highly heterogeneous and contain various pore types, including intergranular, vuggy, and fracture porosity. Engineers and geoscientists often rely on empirical correlations and statistical analysis to overcome this challenge and estimate permeability from FRF measurements in carbonate reservoirs. These correlations are derived from well data and are specific to certain reservoir conditions or regions. Traditionally, rock typing techniques have relied solely on electrical properties, such as resistivity and conductivity, or hydraulic properties, such as permeability and porosity[42,43].

The classification of subsurface rocks is done through the use of electrical properties in electrical rock typing. It helps to bridge the gap between geophysical measurements and geological interpretation[30]. The cementation factor, often denoted by the symbol "m", is a parameter used in petrophysics to describe the cementation level or degree of bonding between mineral grains in a rock formation. It is part of Archie's equation, which relates the formation resistivity factor of a rock to its porosity. A higher cementation factor indicates stronger bonding between grains, leading to lower porosity and increased electrical resistivity[44–47]. Tortuosity refers to the complexity or irregularity of the flow path within a porous medium, such as a rock. In petrophysics, the tortuosity factor ("a") measures how convoluted or twisted the flow path is for fluids and electrical currents within the rock. It is a critical parameter in models describing permeability and electrical conductivity in porous media. Higher tortuosity values indicate more intricate pathways, which can affect the transport of fluid and electrical current through the rock matrix[48–50]. The FRF is a term used in petrophysics and reservoir engineering to describe the relationship between the resistivity of a rock formation and the resistivity of the fluids within it, typically the formation water. The FRF can be defined as follows (Eq. 1):

$$\mathrm{FRF} = \frac{\mathrm{R_o}}{\mathrm{R_w}}, \tag{1}$$

where FRF represents the ratio of the resistivity of the rock saturated with brine (Ro) to the resistivity of the formation water (Rw). Archie introduced a linear relationship, represented on a log–log scale, between FRF and porosity (ϕ). The Eq. (2) explains the relationship between FRF and ϕ[44]:

$$\mathrm{F} = \phi^{-\mathrm{m}}. \tag{2}$$

Rezaee et al.[51] conducted an extensive investigation involving 92 clean carbonate rock samples, with the primary objective of exploring the FRF. To better understand the associated tortuosity and cementation factors, they classified the rock samples into distinct groups based on criteria such as permeability, petro-facies, and reservoir rock types. Their research led them to a notable conclusion: relying solely on the classification of rock samples using these criteria was insufficient for accurately predicting the values of "a" and "m". In response to this

challenge, they introduced a novel parameter termed the Current Zone Indicator (CZI), which was calculated using the following equation:

$$\mathrm{CZI} = \frac{\sqrt{\frac{\phi}{\mathrm{F}}}}{\phi_{\mathrm{N}}}, \tag{3}$$

where ϕ_N represented normalized porosity, and $\sqrt{\frac{\phi}{F}}$ was referred to as the electrical radius indicator (ERI). Their findings strongly supported the notion that grouping rock samples based on CZI was an effective and more reliable method for predicting the "m" and "a" values for each category of samples. In their comprehensive study, the values of "m" ranged from 1.1 to 1.3, while "a" fell within the range of 5 to 19. This innovative approach revolutionized the characterization and categorization of carbonate rock samples, offering enhanced precision for petrophysical analysis and exploration.

Soleymanzadeh et al.[30] introduced another electrical parameter known as the electrical quality index (EQI) with the primary objective of refining the classification of porosity-FRF data and improving the estimation of the cementation factor. The EQI is mathematically expressed as follows:

$$\mathrm{EQI} = \sqrt{\frac{\sigma_o}{\phi} \times \frac{1}{\sigma_w}} = \sqrt{\frac{1}{\mathrm{F}\phi}}. \tag{4}$$

In which, σ_o represents the electrical conductivity of water-saturated rock when the electrical conductivity of the solid matrix is zero, which typically occurs in the case of clean rock samples. σ_w signifies the electrical conductivity of water. Their findings demonstrated that rock samples with similar EQI values exhibited identical electrical behaviour. The researchers applied this innovative parameter to a dataset comprising 112 carbonate samples, which they systematically categorized into nine distinct classes. Each class was associated with a specific equation linking FRF to porosity. Moreover, the research unveiled an intriguing observation: the plots depicting the cementation factor versus porosity yielded linear trends characterized by high determination coefficients.

Mohammadi et al.[52] developed a new electrical rock typing method called the electrical zone indicator (EZI), which offers a more precise determination of reservoir electrical parameters compared to existing methods such as the EQI. The EZI approach involves a modification of EQI, reducing its reliance on porosity as a primary factor. The EZI parameter for each rock sample is calculated by evaluating the ratio of EQI to normalized porosity, as defined in Eq. (5):

$$\mathrm{EZI} = \frac{\mathrm{EQI}}{\phi_{\mathrm{N}}} = \frac{\sqrt{\frac{1}{\mathrm{F}\phi}}}{\frac{\phi}{1-\phi}}. \tag{5}$$

By employing this formulation, EZI is anticipated to exhibit reduced dependence on porosity when compared with the EQI. Consequently, this novel concept was implemented to enhance the classification of rock samples.

Hydraulic rock typing (HRT) is a classification of rocks based on their hydraulic properties. Understanding how fluids, especially hydrocarbons, flow through reservoir rocks is essential, with HRT playing a key role in this process. It considers various petrophysical properties, including porosity, permeability, and relative permeability, to classify rock formations into distinct hydraulic units[53–55]. This approach involves grouping reservoir rocks with similar hydraulic behaviour, enabling a more accurate understanding of fluid flow within the subsurface[56,57]. The flow zone indicator (FZI) is a petrophysical parameter used in the oil and gas industry to classify and characterize subsurface rock formations based on their fluid flow properties. FZI is a critical tool for understanding reservoir quality, fluid distribution, and the potential for hydrocarbon production (Eqs. 6–8)[58,59]. It is primarily used in conjunction with well log data to analyze the flow behavior of reservoirs[60–62].

$$\phi_{\mathrm{N}} = \frac{\phi}{1-\phi}, \tag{6}$$

$$\mathrm{RQI} = 0.0314\sqrt{\frac{\mathrm{k}}{\phi}}, \tag{7}$$

$$\mathrm{FZI} = \frac{\mathrm{RQI}}{\phi_{\mathrm{N}}} = \frac{0.0314\sqrt{\frac{\mathrm{K}}{\phi}}}{\frac{\phi}{1-\phi}}, \tag{8}$$

where ϕ_N represents normalized porosity, RQI and FZI are reservoir quality index and flow zone indicator, respectively.

Xu et al.[63] introduced a new hydraulic rock typing method for reservoirs straddling multiple capillary windows. Their method utilized resistivity-saturation equations and Timur-Tixier's permeability model to establish relationships between petrophysical properties. The study was tested on a gas reservoir in offshore Trinidad, showing improved accuracy in rock typing compared to existing methods. The authors emphasized the importance of considering capillary pressure behaviour in different capillary windows for reliable rock typing.

Mirzaei-Paiaman et al.[54] proposed a new classification of petrophysical rock types into static and dynamic ones. The static rock type was based on primary drainage capillary pressure curves or unique water saturation,

while the dynamic rock type considered fluid flow behaviour. They derived new indices for rock typing, which were tested with core data from a heterogeneous carbonate reservoir. The results demonstrated the superiority of their approach over existing models, emphasizing the importance of rock typing methods that account for wettability and capillary pressure characteristics.

Liu et al.[64] introduced a novel method for petrophysical static rock typing in carbonate reservoirs based on mercury injection capillary pressure curves and principal component analysis. The relationships between petrophysical properties and parameters derived from the capillary pressure curves were established. The approach was applied to a field case in the Mishrif formation, demonstrating superior results compared to traditional methods such as the Winland plot and flow zone indicator.

Sawayama et al.[65] investigated the relationship between hydraulic, electrical, and elastic properties of natural rock fractures under elevated stress conditions. They employed lattice Boltzmann simulation to unveil transitions in three-dimensional flow paths and used finite-element modelling to study the evolution of geophysical properties. The study revealed that electrical resistivity was linked with permeability and flow area irrespective of fracture roughness, while elastic wave velocity depended on roughness. These findings had potential applications in studies of geoengineering developments, seismicity, seismogenic zones, and geothermal reservoirs.

El-Sayed et al.[66] described and evaluated the reservoir quality of Nubia sandstone in south-west Sinai using hydraulic and electric flow units (HFU and EFU). HFU discrimination was based on permeability and porosity relationships, while EFU differentiation relied on resistivity-porosity correlations. A petrographic investigation revealed that the studied samples were mainly quartz arenite, with varying cementation processes that affected reservoir properties. The study provided a semi-empirical relationship between complex mineral IP characteristics and permeability, enhancing the understanding of reservoir characterization.

Barach et al.[67] discussed the importance of petrophysical rock typing for reservoir characterization and field development planning. They examined various approaches based on porosity and permeability relationships, including hydraulic flow unit, global hydraulic element, and Winland R35 methods. The study emphasized integrating geological features with engineering attributes to effectively distribute geological facies in reservoir models. Their proposed workflow enhanced the accuracy of reservoir estimates and forecasts.

Tong et al.[68] proposed a semi-empirical reservoir permeability prediction model based on the modified generalized practical medium theory of induced polarization (MGEMTIP). The model accounted for the effects of various conductive minerals and provided a relationship between complex mineral-induced polarization characteristics and permeability. The study compared the prediction model with two electrical Kozeny-Carman (K-C) models, showing its suitability for low-porosity and low-permeability rocks containing low-resistivity minerals. This model offered a theoretical basis for reservoir permeability prediction based on electromagnetic exploration.

In summary, these studies have contributed significantly to advancing reservoir characterization and rock typing methods, providing valuable insights into understanding reservoir properties, flow behaviour, and the applicability of different approaches in various geological settings. Since over 85% of Iranian reservoirs consist of carbonate rocks, which present unique challenges due to their heterogeneity, the decision was made to focus on carbonate lithology.

In this study, a new approach for rock typing is derived to leverage the strengths of both rock typing methods (electrical and hydraulic), allowing for a more comprehensive and accurate characterization of carbonate reservoir rocks called hydraulic-electric index (HEI). This approach results in the development of distinctive electrical rock types that consider both hydraulic and electrical behaviours, improving the precision of permeability assessment and the overall classification of rocks. Two carbonate datasets have been employed. The first dataset (112 samples) is associated with a study conducted by Ragland[69], and the second dataset (81 samples) pertains to one of the regions in the southwestern part of Iran. These datasets represent diverse lithologies, porosities, and permeabilities, ensuring a comprehensive performance evaluation of the HEI method. The success of the HEI approach holds great promise in revolutionizing reservoir characterization for carbonate formations. The approach can accurately represent the reservoir's heterogeneity and fluid distribution by capturing the interplay between hydraulic conductivity and electrical resistivity. Such insights are invaluable for optimizing production strategies, well placement decisions, and enhanced reservoir management.

Case study

In this study, two sets of samples were employed to demonstrate the improved accuracy in determining the permeability, porosity and FRF offered by the proposed HEI approach. The first set, dataset 1, consists of 112 samples from Ragland's study[69]. The second set, dataset 2, includes 81 samples from an Iranian carbonate reservoir[52]. Stratigraphic information for both sample series is provided below. It is worth noting that both datasets encompass data on permeability, porosity, and FRF, as visually represented in detail in Table 1.

Sample	Porosity	Permeability (mD)	FRF
Dataset 1	$0.013 < \phi < 0.293$	$0.001 < K < 501.390$	$7.215 < FRF < 2323.786$
Dataset 2	$0.030 < \phi < 0.266$	$0.020 < K < 79.349$	$18.580 < FRF < 534$

Table 1. Variation range of porosity, permeability and resistivity for two datasets[52].

Dataset

The dataset 1 is derived from the Tensleep formation, a vast carbonate reservoir in the Bighorn basin spanning Wyoming and Montana in the United States. This geological formation originates from the Pennsylvanian subperiod and predominantly comprises fossil-rich limestone and dolomite sediments formed in a shallow marine shelf environment. Within these samples, a heterogeneous blend of grainstones, packstones, wackestones, and mudstones features intricate intercrystalline, vuggy, and microporous networks. Furthermore, various diagenetic processes, such as fracturing, dissolution, and dolomitization, have further augmented the pore structures within these carbonate rocks. Core plugs have been extracted from depths between 7000 and 8000 feet, displaying 3 to 25% porosities. Additionally, permeabilities exhibit a broad range, varying between 0.02 to 534 milliDarcies (mD), as documented by Ragland[69]. The intricate nature of the pore structures and the presence of multiple pore types in these carbonate samples pose significant challenges when estimating electrical parameters. It is worth noting that the Tensleep formation within the Bighorn Basin is characterized by the following stratigraphic column:

Madison limestone
This layer is identified by its light gray appearance, cherty composition, and micritic limestone deposited in a deep marine basin environment during the Mississippian period.

Amsden formation
The Amsden Formation is distinguished by redbeds, sandstones, siltstones, and limestones. It originated in a tidal flat setting during the Pennsylvanian period.

Tensleep formation
The focal point of our study is fossiliferous limestones and dolomites. It was formed on a shallow marine carbonate shelf during the Pennsylvanian and exhibited wackestone-packstone textures.

Phosphoria formation
Within this layer, phosphate-rich mudrocks, chert, and siltstones could be found. These materials were deposited in a deep marine basin environment during the Permian period.

Goose egg formation
This formation consists of fossiliferous limestones and was deposited in a shallow marine setting during the Permian period.

Dataset 2 originates from the Asmari formation, a giant carbonate reservoir in the southwestern region of Iran. The Asmari formation is characterized by its diverse composition: fossil-bearing limestone, dolomitic limestone, argillaceous limestone, sandstone, and shale. This formation serves as the primary reservoir rock for numerous oil wells in the Zagros region. The Asmari formation is a complex stratigraphic unit consisting of several members and sub-members. The formation is generally divided into two main units: the Lower Asmari and the Upper Asmari.

The Lower Asmari comprises thick sequences of limestone and dolomite, with interbedded layers of marl and shale. This unit is typically characterized by its high degree of heterogeneity, with significant variations in lithology and depositional environment across different regions.

The Upper Asmari, on the other hand, is composed primarily of limestone and marl, with fewer dolomite beds. This unit is generally more homogeneous than the Lower Asmari, with a more consistent lithology and depositional environment.

Within both the Lower and Upper Asmari, several sub-members are distinguished based on lithology, thickness, and depositional environment differences. These include the Khami, Gachsaran, Sarvak, and Pabdeh submembers, among others[70–72].

The Asmari formation is known for its rich fossil content, which has been used to define several biozones within the formation. Biozones are specific assemblages of fossils that characterize intervals of rock, and they are helpful for correlating rocks across different regions. The biozones of the Asmari formation are based primarily on the fossil assemblages of benthic foraminifera, which are single-celled organisms that live on the seafloor. These foraminifera are particularly useful for biostratigraphy because they have a wide geographic distribution and a rapid evolutionary rate[70].

The biozones of the Asmari formation include:

1- Nummulites assemblage zone: This zone is characterized by abundant nummulites, which are large, disc-shaped foraminifera that can reach several centimetres in the lower part of the formation.
2- Assilina assemblage zone: This zone is characterized by abundant Assilina, a genus of benthic foraminifera with a distinctive shell shape. This zone is found in the middle part of the formation.
3- Operculina assemblage zone: This zone is characterized by the presence of abundant Operculina, another genus of benthic foraminifera with a distinctive shell shape. This zone is found in the upper part of the formation[73].

Methodology

The primary objective of this research is to develop and validate the Hydraulic-Electric Index (HEI) for the classification and grouping of carbonate rocks. To do so, first, using Eq. (5) for EZI and the relationships outlined in Eqs. (4) and (6) for EQI and normalized porosity, FRF is calculated as follows:

$$EZI = \frac{EQI}{\phi_N} = \frac{\sqrt{\frac{1}{F\phi}}}{\frac{\phi}{1-\phi}} \rightarrow F = \frac{(1-\phi)^2}{\phi^3} \times \frac{1}{(EZI)^2}, \tag{9}$$

By replacing Eqs. (6) and (7) for RQI and normalized porosity in Eq. (8), permeability can be derived as:

$$FZI = \frac{RQI}{\phi_N} = \frac{0.0314\sqrt{\frac{K}{\phi}}}{\frac{\phi}{1-\phi}} \rightarrow K = 1014\frac{\phi^3}{(1-\phi)^2}(FZI)^2. \tag{10}$$

Equation (11) has been obtained by dividing Eq. (10) by Eq. (9).

$$\frac{K}{F} = 1014\frac{\phi^6}{(1-\phi)^4}(FZI)^2(EZI)^2. \tag{11}$$

For simplifying Eq. (11), the term of $1014\frac{\phi^6}{(1-\phi)^4}$ is replaced by ϕ_{HEI}:

$$\phi_{HEI} = 1014\frac{\varnothing^6}{(1-\varnothing)^4}, \tag{12}$$

Applying logarithm to both sides of Eq. (11) establishes the primary equation for HEI. This logarithmic transformation is often employed to simplify relationships and facilitate a clear understanding of the underlying patterns or trends in the data:

$$log\left(\frac{K}{F}\right) = log\phi_{HEI} + log((FZI)^2.(EZI)^2). \tag{13}$$

After calculating the $\frac{K}{F}$ values by ϕ_{HEI} considering the ranges for each rock type, all samples can be categorized into the desired rock typing classes. Subsequently, by plotting K/F against ϕ_{HEI} on a log–log scale, parallel lines with a unit slope are generated. The intercept of these lines at the point where ϕ_{HEI} equals one essentially represents the mean value $(((FZI)^2.(EZI)^2))$ for each rock type category. This mean value is unique to each category.

Equations (9) to (13) fully provide the required parameters for rock typing using the HEI method. The permeability, FRF, ϕ_{HEI}, and $\frac{K}{F}$ values for all the data are calculated based on Eqs. (9) to (13).

As previously stated, the innovative feature of this new concept is the seamless integration of electrical and hydraulic methods in rock classification. Electrical methods, with their detailed analysis of conductivity and resistivity traits, offer us unmatched insights into the complex electrical features of the rock samples. In parallel, hydraulic techniques effortlessly provide precious information about reservoir rocks' permeability and porosity properties. By cleverly merging these two approaches within the HEI concept, we illuminate a previously unexplored domain of knowledge that comprehensively encompasses the nature of rock types and their fluid flow behaviour within the carbonate reservoirs. It is worth emphasizing that employing the HEI enables us to achieve a more exact and reliable permeability estimation. This important parameter significantly governs the flow behaviour of fluids within reservoir rocks. Furthermore, the HEI approach can unveil concealed insights into the intricate connections between permeability, porosity, and their interdependence with hydroelectric properties, delivering an unparalleled comprehension of the petrophysical attributes of the examined rock samples.

General workflow

Figure 1 demonstrates an overview of the proposed HEI rock typing procedure workflow. After preparing the cores, they should be completely cleaned from any contamination and numbered for each dataset. Now, to start the study, routine and special tests are needed to obtain the porosity, permeability and formation resistivity factor. After obtaining the desired properties, 20% of the data are selected completely randomly to check the efficiency and validity of the studied method. In the next step, using relations 4, 5, 7, 8 and 12, EQI, EZI, RQI, FZI and Φ_{HEI} are obtained, respectively. Then, the HEI concept for rock typing is obtained by dividing $\frac{K}{F}$ by Φ_{HEI} and is plotted on a logarithm-logarithm scale ($\frac{K}{F}$ vs Φ_{HEI}). Linear regression is passed through the obtained lines, and the average $(((FZI)^2.(EZI)^2))$ is obtained for each rock type. Creating tables related to extracted data for each rock type group is better. At the end, the permeability for each core in each rock type is obtained and compared with the laboratory values. All the above steps are also performed for that 20% of the selected samples.

Results and discussion

In this study, the objective is to establish a connection between the electrical and hydraulic properties of rocks so that, by having electrical parameters such as the FRF and determining the desired rock typing, it is possible to estimate hydraulic parameters, especially permeability. Considering the data scatter and the heterogeneity of carbonate rocks, extensive studies were conducted to define a parameter for rock typing the samples. After numerous investigations, it was determined that parameter $((K/F)/(\phi_{HEI}))$ exhibits higher and more acceptable accuracy in rock classification. Therefore, by defining this parameter and assigning it to all the data, its suitable

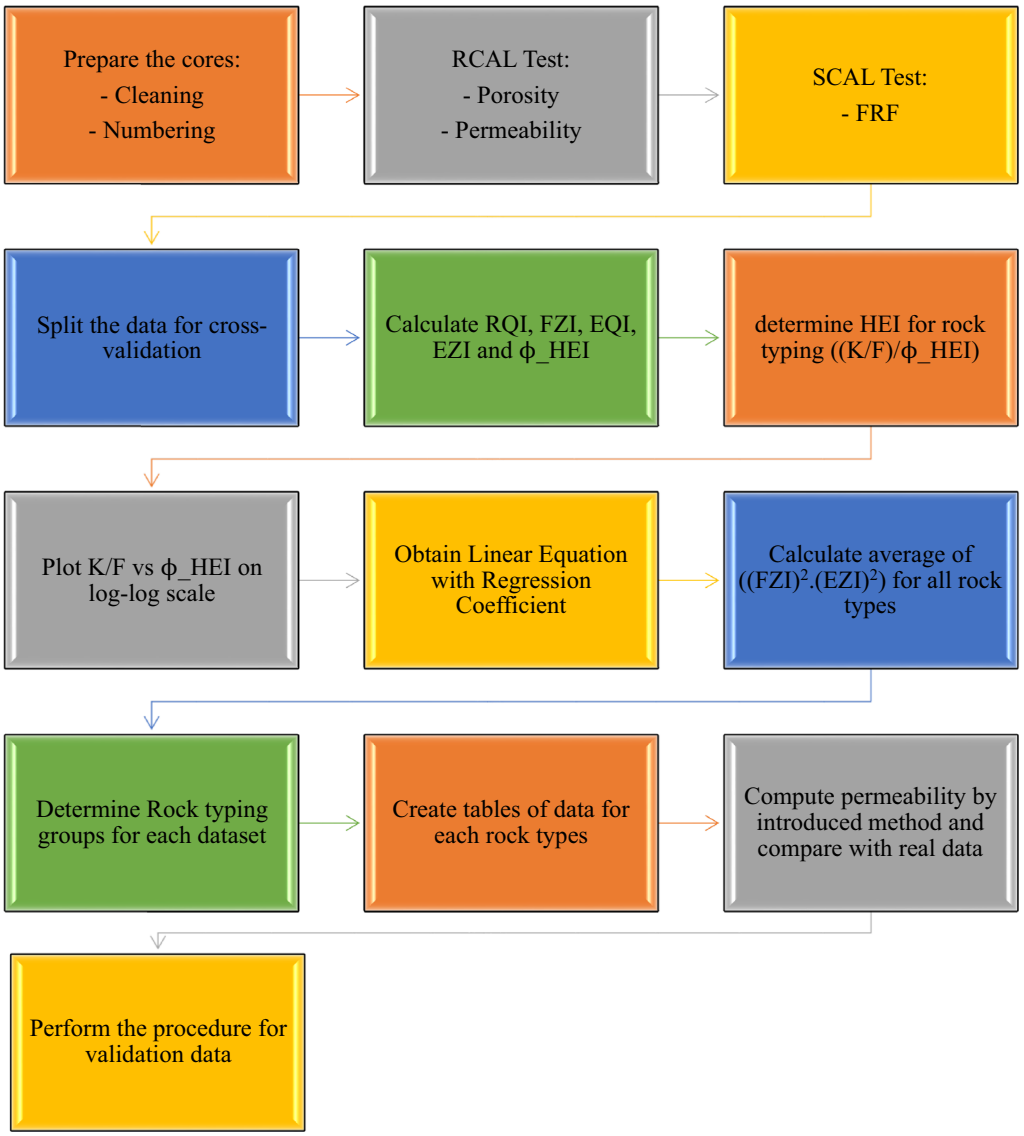

Figure 1. The workflow of the HEI rock typing procedure.

HEI group	Interval $((K/F)/(\phi_{HEI}))$
HEI 1	$0 < (K/F)/(\phi_{HEI}) < 0.1$
HEI 2	$0.1 < (K/F)/(\phi_{HEI}) < 0.2$
HEI 3	$0.2 < (K/F)/(\phi_{HEI}) < 0.4$
HEI 4	$0.4 < (K/F)/(\phi_{HEI}) < 2$
HEI 5	$2 < (K/F)/(\phi_{HEI}) < 4$
HEI 6	$4 < (K/F)/(\phi_{HEI}) < 10$
HEI 7	$10 < (K/F)/(\phi_{HEI}) < 25$
HEI 8	$25 < (K/F)/(\phi_{HEI}) < 200$
HEI 9	$(K/F)/(\phi_{HEI}) > 200$

Table 2. Variation range of division of the $\frac{K}{F}$ values by ϕ_{HEI} for dataset 1.

range for dataset 1 was found to be from 0 to 39,956.236, and for dataset 2, it was from 0 to 993.462. The specified ranges for the selected rock typing intervals for both datasets are presented in Tables 2 and 3, respectively. In the continuation of this section, to assess the performance and efficiency of this method, 20% of the data from each dataset were randomly selected and classified lithologically using the HEI method, and their approximate permeability values were also estimated.

When $\frac{K}{F}$ is plotted against ϕ_{HEI} on a log–log graph, a straight line with a unit slope is obtained for each type of rock. The value of the $((FZI)^2.(EZI)^2)$ can be determined from the intercept of this line at a porosity equal to 1. It is noteworthy that each of these rock types has a unique value of the parameter $((FZI)^2.(EZI)^2)$, which can be easily utilized for data within each category to estimate their permeability. Samples with different $((FZI)^2.(EZI)^2)$ values create parallel lines. The number of these lines corresponds to the number of reservoir rock types. All samples on the same line have uniform pore throats, indicating a single flow unit. With an increase in the numerical average of $((FZI)^2.(EZI)^2)$, reservoir properties improve. According to Eq. (13), the mean value of the parameter $((FZI)^2.(EZI)^2)$ is indeed the unique characteristic for each dataset.

Following Eq. (13) $(\log(\frac{K}{F}) = \log\phi_{HEI} + \log((FZI)^2.(EZI)^2))$, if we assign the vertical axis to $\frac{K}{F}$ and the horizontal axis to ϕ_{HEI} in a log–log scale, adopting the concept of FZI, lines with a consistent slope are formed in parallel. To determine the parameter $((FZI)^2.(EZI)^2)$ in Eq. (13), it is sufficient to read the vertical axis at points where the horizontal axis equals 1. Since each of these parallel lines represents a specific rock type for different samples, the obtained parameter is considered as an average, equal to the classification number of sample groups that is specific and unique for each set of sample classifications (Figs. 2 and 3). In the next step, K/F was graphed against ϕ_{HEI} for each dataset. It should be noted that several parallel lines have been created for both datasets in Figs. 2 and 3, representing the rock typing generated by the HEI method. By obtaining the values of these lines at the point where their horizontal axis equals 1, parameter $((FZI)^2.(EZI)^2)$ can be determined. As mentioned earlier, since this value is unique for samples of each rock type, it is used in an averaged form. Considering the obtained values for all samples, dataset 1 was divided into nine rock types, and dataset 2 was divided into four.

Using the identified number of classes for the samples, the desired line equation can be written for each set and the accuracy of the work can be assessed according to the written equation and the resulting determination coefficient (Tables 4 and 5).

Using Eq. (11), after calculating the parameter $((FZI)^2.(EZI)^2)$, the permeability values are calculated for each dataset based on the relevant rock typing to assess the accuracy and efficiency of the HEI method. Finally, they can be plotted against the actual permeability values in a log–log scale. The determination coefficient (R^2) for all groups demonstrates the accuracy of this method (Figs. 4 and 5).

In the proposed workflow for the HEI method (Fig. 1), 20% of samples are randomly selected for sensitivity analysis (k-fold cross-validation). Characteristics like porosity, permeability, and the formation resistivity factor are determined for all samples. Equations from previous sections are used to calculate parameters RQI, FZI, EQI, EZI and ϕ_{HEI}. Parameter $(\frac{K}{F})/(\phi_{HEI})$ is then determined for all samples and assigned to defined intervals

HEI group	Interval $((K/F)/(\phi_{HEI}))$
HEI 1	$0 < (K/F)/(\phi_{HEI}) < 1$
HEI 2	$1 < (K/F)/(\phi_{HEI}) < 3$
HEI 3	$3 < (K/F)/(\phi_{HEI}) < 10$
HEI 4	$(K/F)/(\phi_{HEI}) > 10$

Table 3. Variation range of division of the $\frac{K}{F}$ values by ϕ_{HEI} for dataset 2.

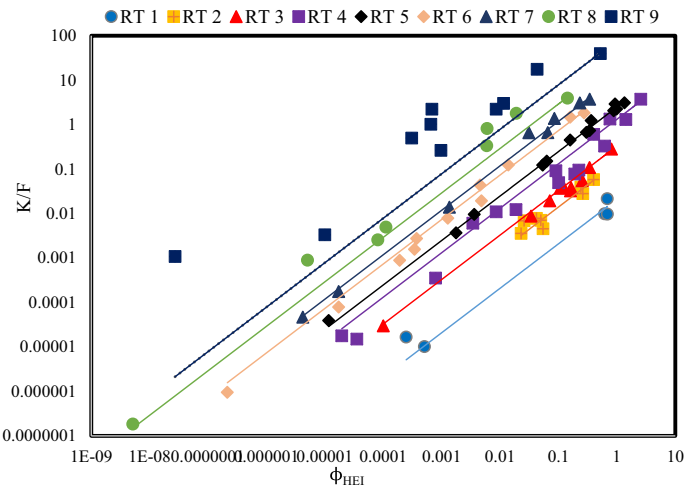

Figure 2. K/F vs ϕ_{HEI} for dataset 1.

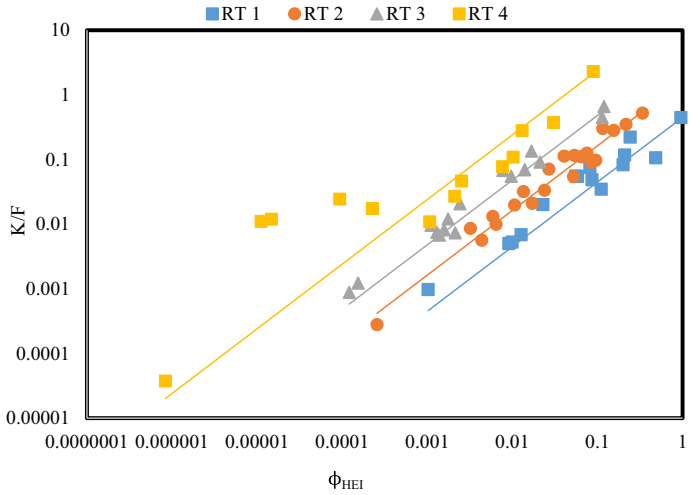

Figure 3. K/F vs ϕ_{HEI} for dataset 2.

Rock type	Equation	Ave $((FZI)^2.(EZI)^2)$	R^2
1	y = 0.0209x	0.0209	0.7392
2	y = 0.1405x	0.1405	0.9535
3	y = 0.3289x	0.3289	0.97
4	y = 1.3186x	1.3186	0.9376
5	y = 2.4828x	2.4828	0.9601
6	y = 7.3669x	7.3669	0.9719
7	y = 11.87x	11.87	0.9695
8	y = 29.133x	29.133	0.8513
9	y = 78.681x	78.681	0.8515

Table 4. The derived equations, the average of HEI rock typing parameters and the determination coefficient for the rock types of dataset 1.

Rock type	Equation	Ave $((FZI)^2.(EZI)^2)$	R^2
1	y = 0.4487x	0.4487	0.8415
2	y = 1.6306x	1.6306	0.9332
3	y = 4.8055x	4.8055	0.9579
4	y = 24.049x	24.049	0.9603

Table 5. The derived equations, the average of HEI rock typing parameters and the determination coefficient for the rock types of dataset 2.

in Tables 2 and 3 for rock types. Next, by plotting $\frac{K}{F}$ against ϕ_{HEI} on a log–log scale, creating parallel lines, and determining parameter $((FZI)^2.(EZI)^2)$ for each rock type, predicted permeability values are obtained and compared with actual measured values. In the final step, the entire process is performed on the selected 20% of data, and determination coefficients are calculated for the accuracy assessment of the proposed method.

Sensitivity analysis (K-fold cross validation)

The last step includes evaluating the method's accuracy through sensitivity coefficient analysis and determining the appropriate sample number for evaluation to assess its efficiency and precision. The recommended approach involves selecting a subset of data, precisely 20% of the entire dataset, at the study's outset. Finally, the obtained method was applied and classifications were performed on these selected data (for 5 folds). Permeability values for these samples were determined and they were compared with the laboratory-derived actual values for each fold. This process allows for a thorough examination of the method's efficiency and accuracy. Utilizing the HEI method involves calculating the K/F vs. ϕ_{HEI} for selected samples using available permeability, porosity, and FRF

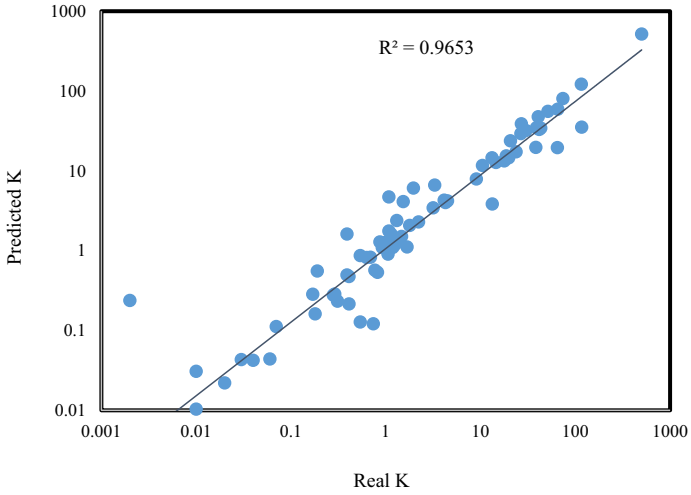

Figure 4. Permeability prediction curve by HEI rock typing method for dataset 1.

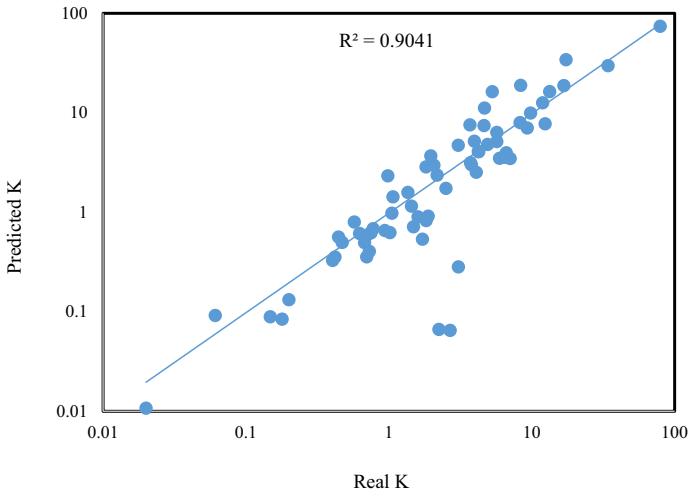

Figure 5. Permeability prediction curve by HEI rock typing method for dataset 2.

data. The results are tabulated in Tables 6 and 7 in the Appendix section, corresponding to dataset 1 and dataset 2, respectively. The analysis then moves on to determine the rock type for each sample, allowing us to identify the parameter (average $((FZI)^2.(EZI)^2)$) for each one. Subsequently, Eq. (11) is applied to derive permeability values for the selected data in Tables 8, 9, 10, 11, 12, 13, 14, 15, 16 and 17 for dataset 1 and dataset 2, respectively. This comparative analysis employs a log–log scale, where the vertical axis represents HEI-derived permeability, and the horizontal axis represents laboratory-measured permeability. As previously explained, predicting permeability for the selected 20% of data for sensitivity analysis is essential. Following the workflow described in Fig. 1, after calculating the permeability for these samples, a comparison with actual permeability values is made on a log–log scale (Figs. 6, 7, 8, 9, 10, 11, 12, 13, 14 and 15 for dataset 1 and 2, respectively). The average of determination coefficients of 0.883 and 0.859 are observed for datasets 1 and 2, respectively. These high determination coefficients underscore the HEI method's precision in the permeability calculation.

Conclusions

- This innovative research presents a study that introduces the hydraulic-electrical index (HEI) approach, a new technique for analyzing rock typing in complex carbonate reservoirs. The study demonstrates that by integrating hydraulic and electrical rock properties, i.e. permeability and formation resistivity factor, a new parameter called HEI is defined; this parameter allows researchers to achieve more precise permeability prediction and enhance the categorization of rock samples.
- An extensive examination of two datasets containing various rock types demonstrates the wide-ranging effectiveness and adaptability of the HEI technique across various geological environments. By incorporating porosity, permeability, and resistivity data, the HEI method generates unique classification indices that

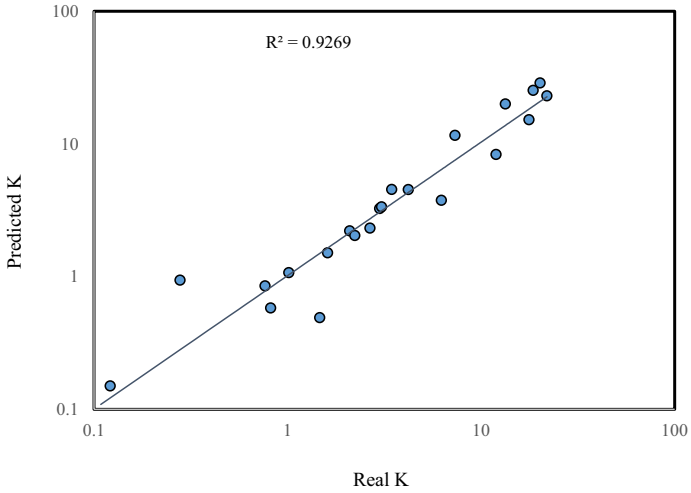

Figure 6. Permeability prediction curve by HEI rock typing method for dataset 1 (fold 1).

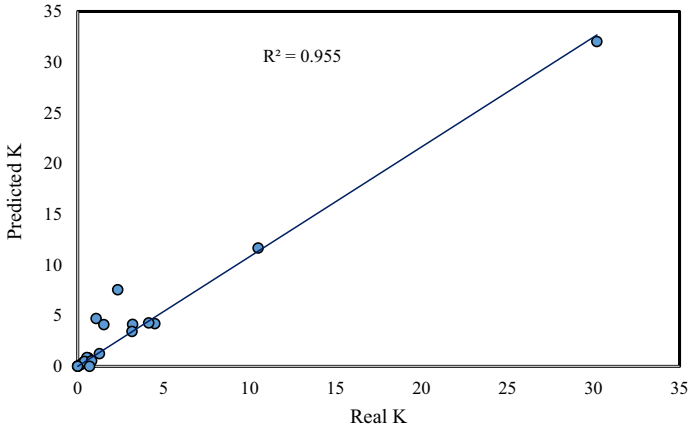

Figure 7. Permeability prediction curve by HEI rock typing method for dataset 1 (fold 2).

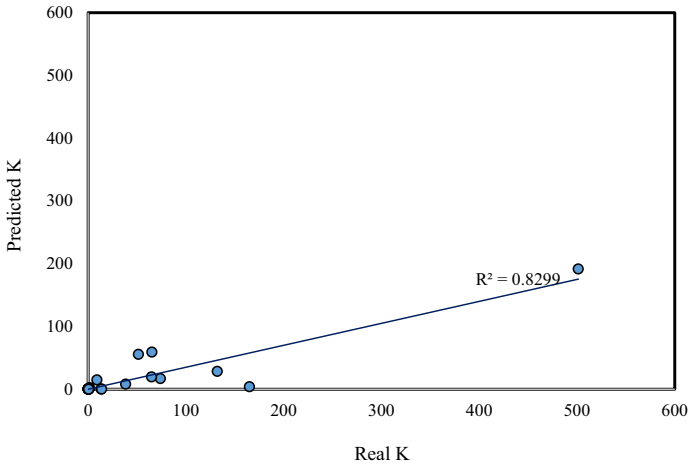

Figure 8. Permeability prediction curve by HEI rock typing method for dataset 1 (fold 3).

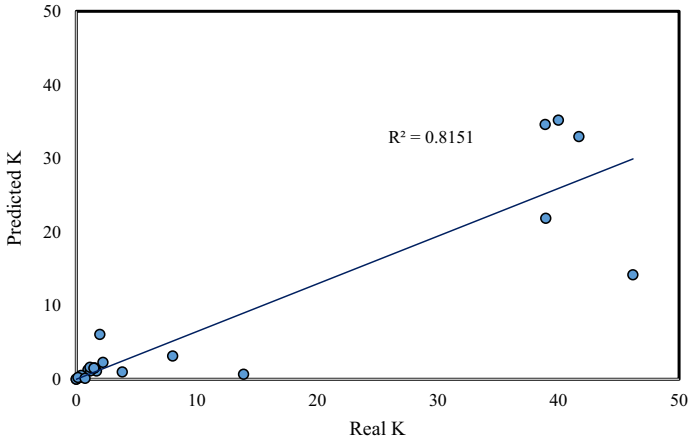

Figure 9. Permeability prediction curve by HEI rock typing method for dataset 1 (fold 4).

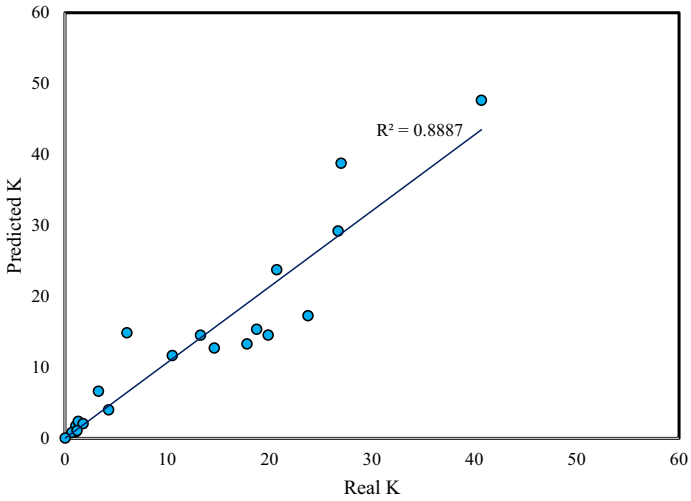

Figure 10. Permeability prediction curve by HEI rock typing method for dataset 1 (fold 5).

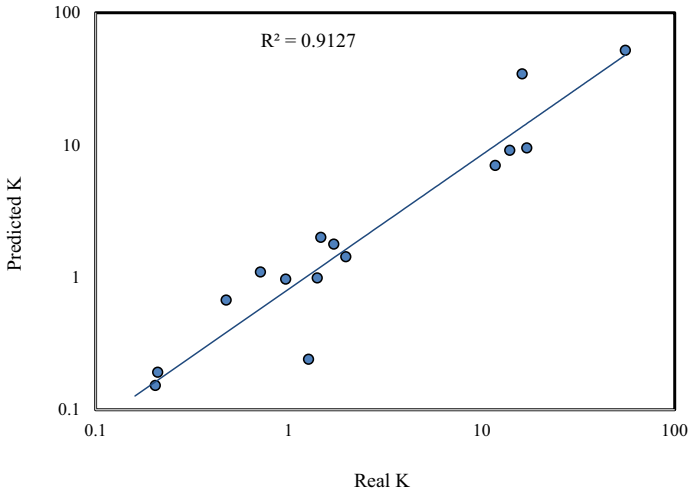

Figure 11. Permeability prediction curve by HEI rock typing method for dataset 2 (fold 1).

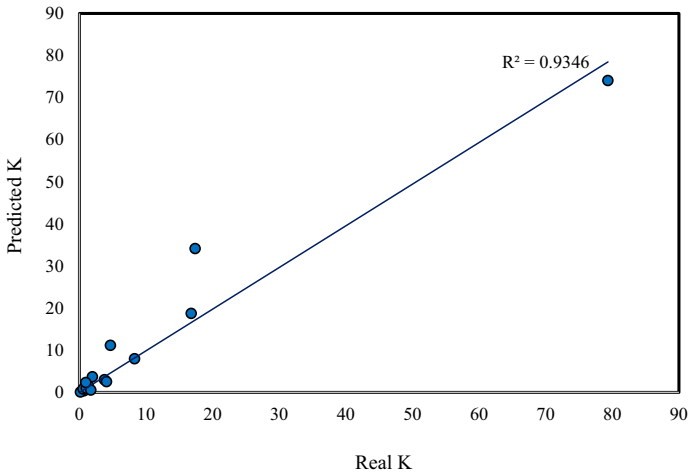

Figure 12. Permeability prediction curve by HEI rock typing method for dataset 2 (fold 2).

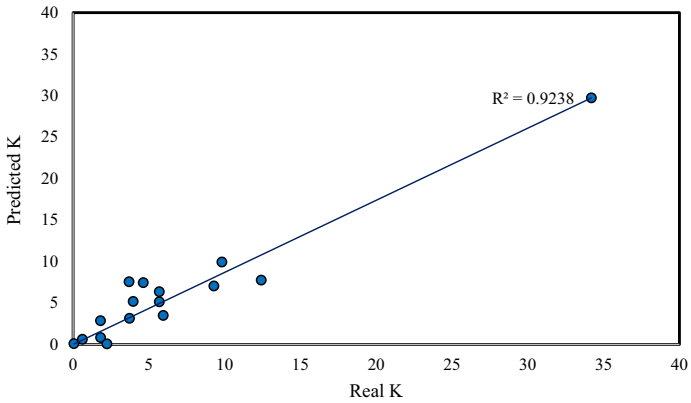

Figure 13. Permeability prediction curve by HEI rock typing method for dataset 2 (fold 3).

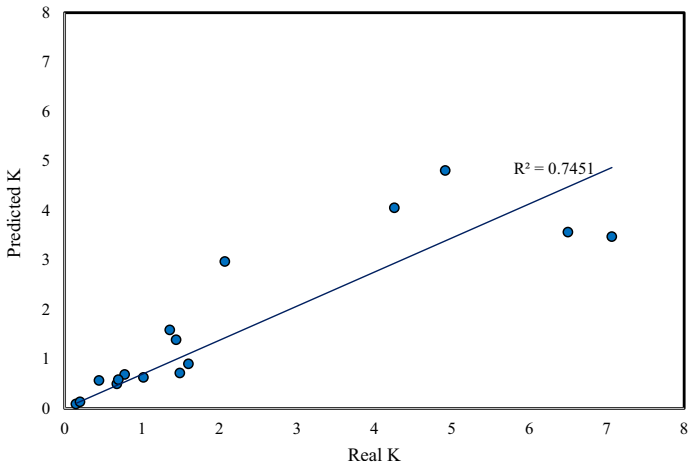

Figure 14. Permeability prediction curve by HEI rock typing method for dataset 2 (fold 4).

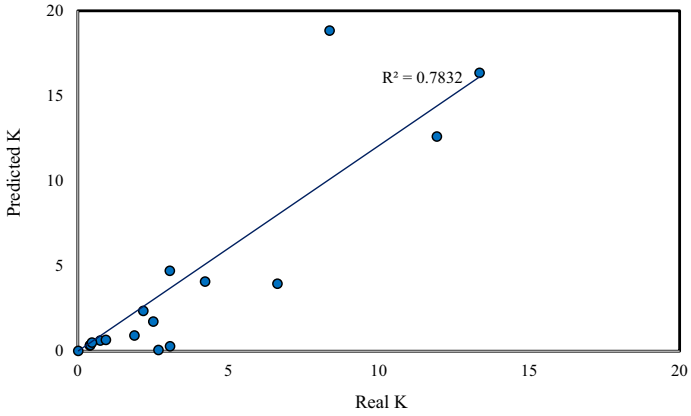

Figure 15. Permeability prediction curve by HEI rock typing method for dataset 2 (fold 5).

successfully differentiate between rock types with similar petrophysical attributes. This integrated process enables the generation of informative graphs and aids in the development of predictive equations for accurately estimating permeability based on HEI values.

- The concept of HEI offers a comprehensive approach to studying carbonate formations by integrating both hydraulic and electrical properties. By incorporating this method, the accuracy of rock typing is enhanced, reducing uncertainty in reservoir characterization. This innovative technique moves beyond conventional methods, providing a more holistic framework for analyzing complex carbonate formations and improving overall understanding of the field.
- The HEI rock typing method was used to predict permeability in two datasets, with 20% of the data being cross-validated. The determination coefficients of 0.914 and 0.860 for dataset 1 and dataset 2, respectively, demonstrate the solid predictive capability of the HEI method in estimating permeability in these geological settings.

Data availability

The corresponding author will make all the data available upon a reasonable request.

Appendix 1

Porosity, permeability, FRF, RQI, FZI, EQI, EZI, K/F and ϕ_{HEI} of samples (except 20% data were used for validation) were used in this study are given in Table 6 (dataset 1) and Table 7 (for Iran) and 8 and 9 for 20% data were used for validation.

Sample no	ϕ	K (mD)	ϕ (%)	FRF	ϕN	RQI	FZI	EQI	EZI	K/F	ϕHEI
1	8.4	0.01	0.084	978.371	0.0917	0.0108	0.1181	0.0093	0.1010	1E−05	0.00051
2	7.5	0.01	0.075	600.6185	0.0811	0.0115	0.1414	0.0112	0.1378	2E−05	0.00025
3	6.5	0.02	0.065	668.7537	0.0695	0.0174	0.2505	0.0099	0.1418	3E−05	0.00010
4	5.5	0.01	0.055	663.1131	0.0582	0.0134	0.2300	0.0091	0.1565	2E−05	0.00004
5	28.15	1.08	0.2815	118.9779	0.3918	0.0615	0.1570	0.0486	0.1242	9E−03	1.89322
6	24.19	0.97	0.2419	97.9166	0.3191	0.0629	0.1971	0.0497	0.1558	1E−02	0.61510
7	24.56	0.87	0.2456	89.3860	0.3256	0.0591	0.1815	0.0524	0.1610	1E−02	0.68707
8	24.55	1.68	0.2455	77.7751	0.3254	0.0821	0.2524	0.0562	0.1727	2E−02	0.68503
9	15.07	0.18	0.1507	50.2696	0.1774	0.0343	0.1934	0.0548	0.3086	4E−03	0.02283
10	15.98	0.39	0.1598	44.5242	0.1902	0.0491	0.2579	0.0599	0.3150	9E−03	0.03388
11	16.91	0.29	0.1691	41.0374	0.2035	0.0411	0.2021	0.0642	0.3154	7E−03	0.04974
12	16.49	0.31	0.1649	39.5248	0.1975	0.0431	0.2180	0.0646	0.3271	8E−03	0.04192
13	17.13	0.17	0.1713	37.2218	0.2067	0.0313	0.1513	0.0678	0.3282	5E−03	0.05432
14	21.47	0.63	0.2147	22.3717	0.2734	0.0538	0.1967	0.0980	0.3583	3E−02	0.26115
15	22.78	1.17	0.2278	20.1449	0.2950	0.0712	0.2412	0.1063	0.3605	6E−02	0.39851
16	5	0.03	0.05	1684.823	0.0526	0.0243	0.4621	0.0054	0.1035	2E−05	0.00002
17	1.3	0.001	0.013	5424.905	0.0132	0.0087	0.6612	0.0015	0.1175	2E−07	0.00000
18	2.4	0.002	0.024	2092.025	0.0246	0.0091	0.3686	0.0034	0.1377	1E−06	0.00000
19	9	0.19	0.09	536.3238	0.0989	0.0456	0.4613	0.0130	0.1310	4E−04	0.00079
20	11.3	0.77	0.113	126.5219	0.1274	0.0820	0.6434	0.0299	0.2346	6E−03	0.00341
21	7.2	0.15	0.072	169.1226	0.0776	0.0453	0.5842	0.0206	0.2659	9E−04	0.00019
22	10.2	0.39	0.102	105.3066	0.1136	0.0614	0.5406	0.0311	0.2740	4E−03	0.00176
23	15.34	0.41	0.1534	59.5526	0.1812	0.0513	0.2833	0.0508	0.2801	7E−03	0.02572
24	8	0.28	0.08	101.7057	0.0870	0.0587	0.6756	0.0280	0.3225	3E−03	0.00037
25	20.04	1.08	0.2004	33.2555	0.2506	0.0729	0.2908	0.0776	0.3097	3E−02	0.16067
26	18.44	3.2	0.1844	34.8259	0.2261	0.1308	0.5785	0.0728	0.3218	9E−02	0.09009
27	18.9	1.25	0.189	33.6253	0.2330	0.0808	0.3465	0.0750	0.3217	4E−02	0.10684
28	17.8	0.69	0.178	35.6148	0.2165	0.0618	0.2855	0.0707	0.3265	2E−02	0.07064
29	20.53	2.34	0.2053	30.0860	0.2583	0.1060	0.4104	0.0826	0.3198	8E−02	0.19035
30	20.1	1.14	0.201	30.0071	0.2516	0.0748	0.2973	0.0818	0.3253	4E−02	0.16407
31	19.24	1.27	0.1924	31.3337	0.2382	0.0807	0.3386	0.0784	0.3289	4E−02	0.12092
32	21.41	1.52	0.2141	27.4900	0.2724	0.0837	0.3071	0.0883	0.3239	6E−02	0.25602
33	18.74	1.53	0.1874	30.9615	0.2306	0.0897	0.3890	0.0778	0.3374	5E−02	0.10073
34	21.23	1.06	0.2123	26.7218	0.2695	0.0702	0.2603	0.0891	0.3307	4E−02	0.24115
35	22.28	2.22	0.2228	20.4499	0.2867	0.0991	0.3458	0.1044	0.3641	1E−01	0.33994
36	24.19	6.06	0.2419	18.3462	0.3191	0.1572	0.4925	0.1148	0.3599	3E−01	0.61510
37	17.1	3.17	0.171	25.7803	0.2063	0.1352	0.6554	0.0814	0.3948	1E−01	0.05368
38	21	1.96	0.21	20.6488	0.2658	0.0959	0.3609	0.1008	0.3794	9E−02	0.22328
39	25.1	4.49	0.251	15.8728	0.3351	0.1328	0.3963	0.1258	0.3752	3E−01	0.80566
40	22.79	9.05	0.2279	14.9737	0.2952	0.1979	0.6704	0.1234	0.4180	6E−01	0.39977
41	4.9	0.41	0.049	2323.786	0.0515	0.0908	1.7628	0.0046	0.0891	2E−04	0.00002
42	4.6	0.06	0.046	1522.777	0.0482	0.0359	0.7437	0.0055	0.1140	4E−05	0.00001
43	11.4	4.28	0.114	446.7837	0.1287	0.1924	1.4953	0.0160	0.1241	1E−02	0.00361
44	4.9	0.07	0.049	885.2355	0.0515	0.0375	0.7284	0.0074	0.1444	8E−05	0.00002
45	14.63	3.29	0.1463	268.6204	0.1714	0.1489	0.8689	0.0233	0.1362	1E−02	0.01872
46	3.9	0.04	0.039	852.2865	0.0406	0.0318	0.7836	0.0068	0.1667	5E−05	0.00000
47	7.9	0.54	0.079	343.1292	0.0858	0.0821	0.9571	0.0152	0.1769	2E−03	0.00034
48	13	1.47	0.13	133.8246	0.1494	0.1056	0.7066	0.0312	0.2086	1E−02	0.00854
49	9.8	1.79	0.098	128.3328	0.1086	0.1342	1.2352	0.0276	0.2543	1E−02	0.00136
50	9.7	0.92	0.097	116.6771	0.1074	0.0967	0.9002	0.0288	0.2684	8E−03	0.00127
51	6.61	0.82	0.0661	165.2043	0.0708	0.1106	1.5626	0.0200	0.2826	5E−03	0.00011
52	11.8	3.82	0.118	87.0496	0.1338	0.1787	1.3354	0.0368	0.2752	4E−02	0.00452
53	11.9	1.31	0.119	67.6733	0.1351	0.1042	0.7713	0.0419	0.3105	2E−02	0.00478
54	20	14.6	0.2	32.3426	0.2500	0.2683	1.0731	0.0786	0.3145	5E−01	0.15844
55	22.3	20.7	0.223	27.9746	0.2870	0.3025	1.0541	0.0893	0.3111	7E−01	0.34212
56	20	43.2	0.2	29.3655	0.2500	0.4615	1.8459	0.0825	0.3301	1E + 00	0.15844

Continued

Sample no	ϕ	K (mD)	ϕ (%)	FRF	ϕN	RQI	FZI	EQI	EZI	K/F	ϕHEI
57	27.1	27	0.271	20.6781	0.3717	0.3134	0.8431	0.1145	0.3080	1E + 00	1.42214
58	29.3	65.3	0.293	17.4662	0.4144	0.4688	1.1311	0.1295	0.3125	4E + 00	2.56783
59	17.5	4.14	0.175	27.4301	0.2121	0.1527	0.7200	0.0799	0.3765	2E–01	0.06287
60	26.9	51.5	0.269	16.6085	0.3680	0.4345	1.1807	0.1273	0.3458	3E + 00	1.34550
61	22.48	23.75	0.2248	19.2063	0.2900	0.3227	1.1130	0.1082	0.3731	1E + 00	0.36238
62	25.4	30.2	0.254	14.6732	0.3405	0.3424	1.0056	0.1316	0.3864	2E + 00	0.87919
63	25.6	41.7	0.256	14.2539	0.3441	0.4008	1.1647	0.1340	0.3895	3E + 00	0.93151
64	21.9	10.5	0.219	15.6241	0.2804	0.2174	0.7754	0.1184	0.4222	7E–01	0.30068
65	24.9	17.8	0.249	13.2761	0.3316	0.2655	0.8007	0.1370	0.4131	1E + 00	0.75976
66	25.8	26.7	0.258	11.9326	0.3477	0.3194	0.9187	0.1470	0.4229	2E + 00	0.98660
67	21.1	38.9	0.211	12.6305	0.2674	0.4263	1.5943	0.1293	0.4833	3E + 00	0.23090
68	18.29	19.87	0.1829	14.3987	0.2238	0.3273	1.4621	0.1127	0.5035	1E + 00	0.08516
69	21.61	13.26	0.2161	7.2160	0.2757	0.2460	0.8922	0.1731	0.6277	2E + 00	0.27348
70	4.02	0.74	0.0402	826.3567	0.0419	0.1347	3.2165	0.0070	0.1665	9E–04	0.00001
71	6.28	1.19	0.0628	466.1542	0.0670	0.1367	2.0398	0.0116	0.1732	3E–03	0.00008
72	13.98	18.74	0.1398	150.993	0.1625	0.3635	2.2369	0.0304	0.1872	1E–01	0.01383
73	12.32	132.2	0.1232	162.1123	0.1405	1.0286	7.3203	0.0276	0.1962	8E–01	0.00600
74	12.29	38.41	0.1229	114.186	0.1401	0.5551	3.9616	0.0328	0.2341	3E–01	0.00590
75	1.71	0.7	0.0171	644.9651	0.0174	0.2009	11.5477	0.0051	0.2960	1E–03	0.00000
76	17.6	40.7	0.176	61.3953	0.2136	0.4775	2.2356	0.0535	0.2507	7E–01	0.06537
77	15.78	38.95	0.1578	59.1812	0.1874	0.4933	2.6329	0.0516	0.2756	7E–01	0.03112
78	4.49	0.54	0.0449	162.2991	0.0470	0.1089	2.3164	0.0166	0.3538	3E–03	0.00001
79	13	117	0.13	52.354	0.1494	0.9420	6.3042	0.0498	0.3335	2E + 00	0.00854
80	8.8	165	0.088	73.8356	0.0965	1.3597	14.0910	0.0345	0.3578	2E + 00	0.00068
81	19.7	116	0.197	29.3434	0.2453	0.7619	3.1058	0.0819	0.3340	4E + 00	0.14255
82	8.74	62.68	0.0874	61.4958	0.0958	0.8409	8.7803	0.0377	0.3936	1E + 00	0.00065
83	9.3	13.34	0.093	50.3504	0.1025	0.3761	3.6677	0.0430	0.4191	3E–01	0.00097
84	22.3	74	0.223	19.8095	0.2870	0.5720	1.9930	0.1061	0.3697	4E + 00	0.34212
85	14.66	46.18	0.1466	25.6586	0.1718	0.5573	3.2442	0.0756	0.4400	2E + 00	0.01898
86	16.55	348.19	0.1655	19.8059	0.1983	1.4403	7.2622	0.0914	0.4609	2E + 01	0.04297
87	23.63	501.39	0.2363	12.6679	0.3094	1.4464	4.6746	0.1366	0.4414	4E + 01	0.51895
88	13.59	64.89	0.1359	21.6193	0.1573	0.6861	4.3627	0.0793	0.5041	3E + 00	0.01146
89	7.76	13.88	0.0776	27.7447	0.0841	0.4199	4.9917	0.0529	0.6286	5E–01	0.00031

Table 6. All of the data about dataset 1 without 20% data for validation.

Sample no	ϕ	K (mD)	ϕ (%)	FRF	ϕN	RQI	FZI	EQI	EZI	K/F	ϕHEI
1	0.1507	0.7	0.0015	34.81	0.1774	0.0677	0.3814	0.4366	2.4606	0.0201	0.0228
2	0.0755	0.061	0.0008	218.82	0.0817	0.0282	0.3456	0.2460	3.0126	0.0003	0.0003
3	0.1344	0.777	0.0013	39.43	0.1553	0.0755	0.4862	0.4344	2.7977	0.0197	0.0106
4	0.1049	1.967	0.0010	72.79	0.1172	0.1360	1.1602	0.3619	3.0880	0.0270	0.0021
5	0.0983	0.624	0.0010	91.92	0.1090	0.0791	0.7257	0.3327	3.0516	0.0068	0.0014
6	0.0696	0.148	0.0007	120.5	0.0748	0.0458	0.6121	0.3453	4.6160	0.0012	0.0002
7	0.0457	2.686	0.0005	242.75	0.0479	0.2407	5.0268	0.3002	6.2695	0.0111	0.0000
8	0.0938	0.179	0.0009	183.55	0.1035	0.0434	0.4191	0.2410	2.3283	0.0010	0.0010
9	0.1393	2.513	0.0014	78.89	0.1618	0.1334	0.8240	0.3017	1.8639	0.0319	0.0135
10	0.1641	5.954	0.0016	52.79	0.1963	0.1891	0.9634	0.3398	1.7307	0.1128	0.0406
11	0.1573	17.384	0.0016	46.61	0.1867	0.3301	1.7684	0.3693	1.9785	0.3730	0.0305
12	0.1796	4.917	0.0018	39.26	0.2189	0.1643	0.7505	0.3766	1.7202	0.1252	0.0751
13	0.1911	12.421	0.0019	41.18	0.2362	0.2532	1.0715	0.3565	1.5089	0.3016	0.1154
14	0.0944	0.985	0.0009	90.51	0.1042	0.1014	0.9730	0.3421	3.2819	0.0109	0.0011
15	0.1439	6.64	0.0014	49.14	0.1681	0.2133	1.2690	0.3761	2.2373	0.1351	0.0168
16	0.2125	7.067	0.0021	31.86	0.2698	0.1811	0.6711	0.3843	1.4243	0.2218	0.2428
17	0.2091	9.827	0.0021	28.12	0.2644	0.2153	0.8142	0.4124	1.5599	0.3495	0.2166
18	0.1907	13.357	0.0019	29.92	0.2356	0.2628	1.1152	0.4186	1.7767	0.4464	0.1137
19	0.1544	4.093	0.0015	57.58	0.1826	0.1617	0.8854	0.3354	1.8368	0.0711	0.0269
20	0.1003	1.052	0.0010	129.18	0.1115	0.1017	0.9122	0.2778	2.4920	0.0081	0.0016
21	0.1385	16.809	0.0014	60.02	0.1608	0.3459	2.1517	0.3468	2.1574	0.2801	0.0130
22	0.1229	0.676	0.0012	51.37	0.1401	0.0736	0.5256	0.3980	2.8403	0.0132	0.0059
23	0.1079	3.971	0.0011	85.16	0.1210	0.1905	1.5749	0.3299	2.7275	0.0466	0.0025
24	0.102	0.938	0.0010	77.62	0.1136	0.0952	0.8383	0.3554	3.1289	0.0121	0.0018
25	0.1444	1.07	0.0014	51.03	0.1688	0.0855	0.5065	0.3684	2.1828	0.0210	0.0172
26	0.2226	11.936	0.0022	22.89	0.2863	0.2299	0.8030	0.4430	1.5472	0.5215	0.3378
27	0.1833	1.442	0.0018	29.67	0.2244	0.0881	0.3924	0.4288	1.9106	0.0486	0.0865
28	0.1335	8.37	0.0013	76.9	0.1541	0.2486	1.6138	0.3121	2.0257	0.1088	0.0102
29	0.1756	4.259	0.0018	38.64	0.2130	0.1546	0.7260	0.3839	1.8023	0.1102	0.0644
30	0.1279	4.678	0.0013	60.45	0.1467	0.1899	1.2949	0.3596	2.4522	0.0774	0.0077
31	0.2068	2.18	0.0021	26.27	0.2607	0.1019	0.3910	0.4290	1.6456	0.0830	0.2004
32	0.2569	8.29	0.0026	18.58	0.3457	0.1784	0.5160	0.4577	1.3240	0.4462	0.9559
33	0.1312	0.404	0.0013	80.51	0.1510	0.0551	0.3649	0.3077	2.0375	0.0050	0.0091
34	0.1719	1.826	0.0017	33.03	0.2076	0.1023	0.4930	0.4197	2.0217	0.0553	0.0556
35	0.1072	1.6	0.0011	77.24	0.1201	0.1213	1.0103	0.3475	2.8943	0.0207	0.0024
36	0.0643	3.07	0.0006	125.58	0.0687	0.2170	3.1573	0.3519	5.1211	0.0244	0.0001
37	0.1829	3.06	0.0018	33.95	0.2238	0.1284	0.5738	0.4013	1.7928	0.0901	0.0852
38	0.0949	0.731	0.0009	76.16	0.1049	0.0871	0.8312	0.3720	3.5476	0.0096	0.0011
39	0.1517	1.36	0.0015	40.72	0.1788	0.0940	0.5257	0.4023	2.2499	0.0334	0.0239
40	0.1704	1.82	0.0017	33.48	0.2054	0.1026	0.4996	0.4187	2.0383	0.0544	0.0524
41	0.1817	1.886	0.0018	24.99	0.2220	0.1012	0.4556	0.4693	2.1135	0.0755	0.0814
42	0.1995	5.7	0.0020	20.21	0.2492	0.1678	0.6735	0.4980	1.9983	0.2820	0.1557
43	0.1731	1.49	0.0017	27.26	0.2093	0.0921	0.4401	0.4604	2.1991	0.0547	0.0583
44	0.074	1.72	0.0007	98.34	0.0799	0.1514	1.8943	0.3707	4.6387	0.0175	0.0002
45	0.1245	0.472	0.0012	47.5	0.1422	0.0611	0.4299	0.4112	2.8917	0.0099	0.0064
46	0.0973	0.695	0.0010	93.1	0.1078	0.0839	0.7786	0.3323	3.0825	0.0075	0.0013
47	0.1841	79.349	0.0018	34.56	0.2256	0.6519	2.8891	0.3964	1.7570	2.2960	0.0891
48	0.1325	3.732	0.0013	67.64	0.1527	0.1666	1.0911	0.3340	2.1870	0.0552	0.0097
49	0.14	4.232	0.0014	60.84	0.1628	0.1726	1.0605	0.3426	2.1048	0.0696	0.0140
50	0.1174	0.445	0.0012	78.98	0.1330	0.0611	0.4596	0.3284	2.4689	0.0056	0.0044
51	0.1051	0.573	0.0011	77.96	0.1174	0.0733	0.6243	0.3494	2.9746	0.0074	0.0021
52	0.0478	2.244	0.0005	187.79	0.0502	0.2151	4.2858	0.3338	6.6489	0.0120	0.0000
53	0.19	2.07	0.0019	59.7	0.2346	0.1036	0.4418	0.2969	1.2658	0.0347	0.1108
54	0.138	0.75	0.0014	109	0.1601	0.0732	0.4572	0.2578	1.6106	0.0069	0.0127
55	0.03	0.02	0.0003	534	0.0309	0.0256	0.8290	0.2498	8.0783	0.0000	0.0000
56	0.112	1.02	0.0011	119	0.1261	0.0948	0.7513	0.2739	2.1718	0.0086	0.0032

Continued

Sample no	ϕ	K (mD)	ϕ (%)	FRF	ϕN	RQI	FZI	EQI	EZI	K/F	ϕHEI
57	0.192	34.2	0.0019	51.9	0.2376	0.4191	1.7636	0.3168	1.3331	0.6590	0.1192
58	0.133	0.42	0.0013	79.5	0.1534	0.0558	0.3637	0.3075	2.0047	0.0053	0.0099
59	0.208	3.78	0.0021	32.1	0.2626	0.1339	0.5097	0.3870	1.4736	0.1178	0.2087
60	0.234	3.7	0.0023	34.8	0.3055	0.1249	0.4087	0.3504	1.1471	0.1063	0.4835
61	0.128	6.5	0.0013	96.1	0.1468	0.2238	1.5244	0.2851	1.9424	0.0676	0.0077
62	0.186	4.64	0.0019	47.7	0.2285	0.1568	0.6863	0.3357	1.4693	0.0973	0.0956
63	0.149	5.7	0.0015	62.5	0.1751	0.1942	1.1092	0.3277	1.8716	0.0912	0.0212
64	0.067	0.2	0.0007	227	0.0718	0.0543	0.7555	0.2564	3.5707	0.0009	0.0001
65	0.171	9.3	0.0017	80.4	0.2063	0.2316	1.1226	0.2697	1.3075	0.1157	0.0537

Table 7. All of the data about dataset 2 without 20% data for validation.

Sample no	ϕ	K (mD)	ϕ (%)	FRF	ϕN	RQI	FZI	EQI	EZI	K/F	ϕHEI
1	23.6	1.07	0.2360	94.47724	0.3089	0.0669	0.2164	0.0500	0.1618	0.0113	0.5142
2	20.72	0.85	0.2072	26.83771	0.2614	0.0636	0.2433	0.0879	0.3362	0.0317	0.2031
3	24.11	4.54	0.2411	40.96994	0.3177	0.1363	0.4289	0.0767	0.2415	0.1108	0.6005
4	9.1	0.07	0.0910	390.8291	0.1001	0.0275	0.2751	0.0153	0.1524	0.0002	0.0008
5	17.76	0.58	0.1776	35.78105	0.2160	0.0567	0.2628	0.0705	0.3262	0.0162	0.0696
6	21.51	2.21	0.2151	24.06769	0.2740	0.1006	0.3673	0.0945	0.3450	0.0918	0.2646
7	23.14	3.26	0.2314	20.38973	0.3011	0.1179	0.3915	0.1065	0.3538	0.1599	0.4461
8	14.6	0.49	0.1460	60.24603	0.1710	0.0575	0.3365	0.0492	0.2880	0.0081	0.0185
9	24.1	8.33	0.2410	15.14773	0.3175	0.1846	0.5814	0.1261	0.3972	0.5499	0.5987
10	14.74	2.32	0.1474	102.8575	0.1729	0.1246	0.7206	0.0379	0.2190	0.0226	0.0197
11	24.9	28.8	0.2490	20.14695	0.3316	0.3377	1.0185	0.1112	0.3353	1.4295	0.7598
12	24.6	20	0.2460	14.56512	0.3263	0.2831	0.8678	0.1300	0.3983	1.3731	0.6953
13	6.7	0.15	0.0670	403.7513	0.0718	0.0470	0.6543	0.0129	0.1794	0.0004	0.0001
14	13.9	1.51	0.1390	48.78214	0.1614	0.1035	0.6411	0.0534	0.3306	0.0310	0.0133
15	15.8	3.35	0.1580	39.32533	0.1876	0.1446	0.7705	0.0634	0.3378	0.0852	0.0314
16	21.6	15.2	0.2160	26.15854	0.2755	0.2634	0.9561	0.0909	0.3298	0.5811	0.2726
17	22.8	25.3	0.2280	18.67622	0.2953	0.3308	1.1200	0.1105	0.3741	1.3547	0.4010
18	11.79	3.76	0.1179	188.2744	0.1337	0.1773	1.3267	0.0250	0.1872	0.0200	0.0045
19	13	4.53	0.1300	66.87699	0.1494	0.1854	1.2405	0.0441	0.2951	0.0677	0.0085
20	12	2.04	0.1200	59.86599	0.1364	0.1295	0.9494	0.0448	0.3283	0.0341	0.0050
21	17.8	23	0.1780	26.10395	0.2165	0.3569	1.6483	0.0826	0.3813	0.8811	0.0706
22	10.5	11.6	0.1050	118.8718	0.1173	0.3300	2.8132	0.0297	0.2533	0.0976	0.0021
23	5.95	0.94	0.0595	61.54676	0.0633	0.1248	1.9728	0.0311	2.7275	0.0153	0.0001

Table 8. All of the data about dataset 1 selected data for validation (fold 1).

Sample no	ϕ	K (mD)	ϕ (%)	FRF	ϕN	RQI	FZI	EQI	EZI	K/F	ϕHEI
1	8.4	0.01	0.084	978.371	0.0917	0.0108	0.1181	0.0093	0.1010	0.0000	0.0005
2	28.15	1.08	0.2815	118.9779	0.3918	0.0615	0.1570	0.0486	0.1242	0.0091	1.8932
3	15.07	0.18	0.1507	50.2696	0.1774	0.0343	0.1934	0.0548	0.3086	0.0036	0.0228
4	16.91	0.29	0.1691	41.0374	0.2035	0.0411	0.2021	0.0642	0.3154	0.0071	0.0497
5	21.47	0.63	0.2147	22.3717	0.2734	0.0538	0.1967	0.0980	0.3583	0.0282	0.2611
6	19.24	1.27	0.1924	31.3337	0.2382	0.0807	0.3386	0.0784	0.3289	0.0405	0.1209
7	25.1	4.49	0.251	15.8728	0.3351	0.1328	0.3963	0.1258	0.3752	0.2829	0.8057
8	6.5	0.02	0.065	668.753	0.0695	0.0174	0.2505	0.0099	0.1418	0.0000	0.0001
9	11.3	0.77	0.113	126.5219	0.1274	0.0820	0.6434	0.0299	0.2346	0.0061	0.0034
10	18.44	3.2	0.1844	34.8259	0.2261	0.1308	0.5785	0.0728	0.3218	0.0919	0.0901
11	20.53	2.34	0.2053	30.086	0.2583	0.1060	0.4104	0.0826	0.3198	0.0778	0.1904
12	18.74	1.53	0.1874	30.9615	0.2306	0.0897	0.3890	0.0778	0.3374	0.0494	0.1007
13	10.2	0.39	0.102	105.3066	0.1136	0.0614	0.5406	0.0311	0.2740	0.0037	0.0018
14	17.1	3.17	0.171	25.7803	0.2063	0.1352	0.6554	0.0814	0.3948	0.1230	0.0537
15	17.5	4.14	0.175	27.4301	0.2121	0.1527	0.7200	0.0799	0.3765	0.1509	0.0629
16	21.9	10.5	0.219	15.6241	0.2804	0.2174	0.7754	0.1184	0.4222	0.6720	0.3007
17	25.4	30.2	0.254	14.6732	0.3405	0.3424	1.0056	0.1316	0.3864	2.0582	0.8792
18	7.9	0.54	0.079	343.1292	0.0858	0.0821	0.9571	0.0152	0.1769	0.0016	0.0003
19	4.9	0.41	0.049	2323.786	0.0515	0.0908	1.7628	0.0046	0.0891	0.0002	0.0000
20	6.61	0.82	0.0661	165.2043	0.0708	0.1106	1.5626	0.0200	0.2826	0.0050	0.0001
21	1.71	0.7	0.0171	644.9561	0.0174	0.2009	11.5477	0.0051	0.2960	0.0011	0.0000
22	1.3	0.001	0.013	5424.905	0.0132	0.0087	0.6612	0.0015	0.1175	0.0000	0.0000

Table 9. All of the data about dataset 1 selected data for validation (fold 2).

Sample no	ϕ	K (mD)	ϕ (%)	FRF	ϕN	RQI	FZI	EQI	EZI	K/F	ϕHEI
1	24.56	0.87	0.2456	89.386	0.3256	0.0591	0.1815	0.0524	0.1610	0.0097	0.6871
2	17.13	0.17	0.1713	37.221	0.2067	0.0313	0.1513	0.0678	0.3282	0.0046	0.0543
3	9.7	0.92	0.097	116.677	0.1074	0.0967	0.9002	0.0288	0.2684	0.0079	0.0013
4	21.41	1.52	0.2141	27.49	0.2724	0.0837	0.3071	0.0883	0.3239	0.0553	0.2560
5	18.9	1.25	0.189	33.625	0.2330	0.0808	0.3465	0.0750	0.3217	0.0372	0.1068
6	15.98	0.39	0.1598	44.524	0.1902	0.0491	0.2579	0.0599	0.3150	0.0088	0.0339
7	5	0.03	0.05	1684.823	0.0526	0.0243	0.4621	0.0054	0.1035	0.0000	0.0000
8	29.3	65.3	0.293	17.466	0.4144	0.4688	1.1311	0.1295	0.3125	3.7387	2.5678
9	5.5	0.01	0.055	663.113	0.0582	0.0134	0.2300	0.0091	0.1565	0.0000	0.0000
10	9	0.19	0.09	536.323	0.0989	0.0456	0.4613	0.0130	0.1310	0.0004	0.0008
11	22.79	9.05	0.2279	14.973	0.2952	0.1979	0.6704	0.1234	0.4180	0.6044	0.3998
12	26.9	51.5	0.269	16.608	0.3680	0.4345	1.1807	0.1273	0.3458	3.1009	1.3455
13	22.3	74	0.223	19.809	0.2870	0.5720	1.9930	0.1061	0.3697	3.7357	0.3421
14	9.3	13.34	0.093	50.35	0.1025	0.3761	3.6677	0.0430	0.4191	0.2649	0.0010
15	7.76	13.88	0.0776	27.744	0.0841	0.4199	4.9917	0.0529	0.6286	0.5003	0.0003
16	8	0.28	0.08	101.705	0.0870	0.0587	0.6756	0.0280	0.3225	0.0028	0.0004
17	4.6	0.06	0.046	1522.777	0.0482	0.0359	0.7437	0.0055	0.1140	0.0000	0.0000
18	4.9	0.07	0.049	885.235	0.0515	0.0375	0.7284	0.0074	0.1444	0.0001	0.0000
19	12.29	38.41	0.1229	114.186	0.1401	0.5551	3.9616	0.0328	0.2341	0.3364	0.0059
20	4.49	0.54	0.0449	162.299	0.0470	0.1089	2.3164	0.0166	0.3538	0.0033	0.0000
21	12.32	132.2	0.1232	162.112	0.1405	1.0286	7.3203	0.0276	0.1962	0.8155	0.0060
22	23.63	501.39	0.2363	12.667	0.3094	1.4464	4.6746	0.1366	0.4414	39.5824	0.5190
23	8.8	165	0.088	73.835	0.0965	1.3597	14.0910	0.0345	0.3578	2.2347	0.0007
24	13.59	64.89	0.1359	21.619	0.1573	0.6861	4.3627	0.0793	0.5041	3.0015	0.0115

Table 10. All of the data about dataset 1 selected data for validation (fold 3).

Sample no	ϕ	K (mD)	ϕ (%)	FRF	ϕN	RQI	FZI	EQI	EZI	K/F	ϕHEI
1	7.5	0.01	0.075	600.618	0.0811	0.0115	0.1414	0.0112	0.1378	0.0000	0.0002
2	24.19	0.97	0.2419	97.916	0.3191	0.0629	0.1971	0.0497	0.1558	0.0099	0.6151
3	24.55	1.68	0.2455	77.775	0.3254	0.0821	0.2524	0.0562	0.1727	0.0216	0.6850
4	16.49	0.31	0.1649	39.524	0.1975	0.0431	0.2180	0.0646	0.3271	0.0078	0.0419
5	22.78	1.17	0.2278	20.144	0.2950	0.0712	0.2412	0.1063	0.3605	0.0581	0.3985
6	15.34	0.41	0.1534	59.552	0.1812	0.0513	0.2833	0.0508	0.2801	0.0069	0.0257
7	20.1	1.14	0.201	30.007	0.2516	0.0748	0.2973	0.0818	0.3253	0.0380	0.1641
8	22.28	2.22	0.2228	20.449	0.2867	0.0991	0.3458	0.1044	0.3641	0.1086	0.3399
9	20	1.51	0.2	29.365	0.2500	0.0863	0.3451	0.0825	0.3301	0.0514	0.1584
10	21	1.96	0.21	20.648	0.2658	0.0959	0.3609	0.1008	0.3794	0.0949	0.2233
11	13	1.47	0.13	133.824	0.1494	0.1056	0.7066	0.0312	0.2086	0.0110	0.0085
12	11.8	3.82	0.118	87.049	0.1338	0.1787	1.3354	0.0368	0.2752	0.0439	0.0045
13	25.6	41.7	0.256	14.253	0.3441	0.4008	1.1647	0.1340	0.3895	2.9257	0.9315
14	2.4	0.002	0.024	2092.025	0.0246	0.0091	0.3686	0.0034	0.1377	0.0000	0.0000
15	7.2	0.15	0.072	169.122	0.0776	0.0453	0.5842	0.0206	0.2659	0.0009	0.0002
16	21.1	38.9	0.211	12.63	0.2674	0.4263	1.5943	0.1293	0.4833	3.0800	0.2309
17	15.78	38.95	0.1578	59.181	0.1874	0.4933	2.6329	0.0516	0.2756	0.6582	0.0311
18	14.66	46.18	0.1466	25.658	0.1718	0.5573	3.2442	0.0756	0.4400	1.7998	0.0190
19	4.02	0.74	0.0402	826.356	0.0419	0.1347	3.2165	0.0070	0.1665	0.0009	0.0000
20	13	117	0.13	52.354	0.1494	0.9420	6.3042	0.0498	0.3335	2.2348	0.0085
21	8.74	62.68	0.0874	61.495	0.0958	0.8409	8.7803	0.0377	0.3936	1.0193	0.0007
22	7.76	13.88	0.0776	27.744	0.0841	0.4199	4.9917	0.0529	0.6286	0.5003	0.0003

Table 11. All of the data about dataset 1 selected data for validation (fold 4).

Sample no	ϕ	K (mD)	ϕ (%)	FRF	ϕN	RQI	FZI	EQI	EZI	K/F	ϕHEI
1	21.23	1.06	0.2123	26.721	0.2695	0.0702	0.2603	0.0891	0.3307	0.0397	0.2412
2	20.04	1.08	0.2004	33.255	0.2506	0.0729	0.2908	0.0776	0.3097	0.0325	0.1607
3	17.8	0.69	0.178	35.614	0.2165	0.0618	0.2855	0.0707	0.3265	0.0194	0.0706
4	14.63	3.29	0.1463	268.62	0.1714	0.1489	0.8689	0.0233	0.1362	0.0122	0.0187
5	24.19	6.06	0.2419	18.346	0.3191	0.1572	0.4925	0.1148	0.3599	0.3303	0.6151
6	27.1	27	0.271	20.678	0.3717	0.3134	0.8431	0.1145	0.3080	1.3057	1.4221
7	24.9	17.8	0.249	13.276	0.3316	0.2655	0.8007	0.1370	0.4131	1.3408	0.7598
8	11.4	4.28	0.114	446.783	0.1287	0.1924	1.4953	0.0160	0.1241	0.0096	0.0036
9	20	14.6	0.2	32.342	0.2500	0.2683	1.0731	0.0786	0.3146	0.4514	0.1584
10	22.3	20.7	0.223	27.974	0.2870	0.3025	1.0541	0.0893	0.3111	0.7400	0.3421
11	22.48	23.75	0.2248	19.206	0.2900	0.3227	1.1130	0.1082	0.3731	1.2366	0.3624
12	21.9	10.5	0.219	15.624	0.2804	0.2174	0.7754	0.1184	0.4222	0.6720	0.3007
13	25.8	26.7	0.258	11.932	0.3477	0.3194	0.9187	0.1470	0.4229	2.2377	0.9866
14	11.9	1.31	0.119	67.673	0.1351	0.1042	0.7713	0.0419	0.3105	0.0194	0.0048
15	21.61	13.26	0.2161	7.216	0.2757	0.2460	0.8922	0.1731	0.6277	1.8376	0.2735
16	13.98	18.74	0.1398	150.993	0.1625	0.3635	2.2369	0.0304	0.1872	0.1241	0.0138
17	17.6	40.7	0.176	61.395	0.2136	0.4775	2.2356	0.0535	0.2507	0.6629	0.0654
18	3.9	0.04	0.039	852.286	0.0406	0.0318	0.7836	0.0068	0.1667	0.0000	0.0000
19	9.8	1.79	0.098	128.332	0.1086	0.1342	1.2352	0.0276	0.2543	0.0139	0.0014
20	18.29	19.87	0.1829	14.398	0.2238	0.3273	1.4621	0.1127	0.5035	1.3801	0.0852
21	6.28	1.19	0.0628	466.154	0.0670	0.1367	2.0398	0.0116	0.1732	0.0026	0.0001

Table 12. All of the data about dataset 1 selected data for validation (fold 5).

Sample no	ϕ	K (mD)	ϕ (%)	FRF	ϕN	RQI	FZI	EQI	EZI	K/F	ϕHEI
1	0.1683	1.408	0.0017	45.78	0.2024	0.0908	0.4488	0.3602	1.7803	0.0308	0.0482
2	0.2043	1.715	0.0020	21.6	0.2568	0.0910	0.3543	0.476	1.8540	0.0794	0.1839
3	0.094	0.16	0.0009	176	0.1038	0.0410	0.3948	0.2458	2.3696	0.0009	0.0010
4	0.0828	0.204	0.0008	202.52	0.0903	0.0493	0.5460	0.2442	2.7051	0.0010	0.0005
5	0.1507	1.979	0.0015	38.47	0.1774	0.1138	0.6413	0.4153	2.3406	0.0514	0.0228
6	0.1255	0.475	0.0013	60.94	0.1435	0.0611	0.4257	0.3615	2.5197	0.0078	0.0068
7	0.1346	0.715	0.0013	62.57	0.1555	0.0724	0.4653	0.3445	2.2155	0.0114	0.0108
8	0.1634	1.47	0.0016	31.22	0.1953	0.0942	0.4822	0.4427	2.2669	0.0471	0.0394
9	0.1621	14.001	0.0016	50.8	0.1935	0.2918	1.5084	0.3484	1.8013	0.2756	0.0373
10	0.104	0.966	0.0010	101.31	0.1161	0.0957	0.8245	0.308	2.6542	0.0095	0.0020
11	0.1675	17.137	0.0017	42.39	0.2012	0.3176	1.5786	0.3752	1.8652	0.4043	0.0466
12	0.1643	11.769	0.0016	35.69	0.1966	0.2658	1.3517	0.4129	2.1005	0.3298	0.0409
13	0.069	0.21	0.0007	274	0.0741	0.0548	0.7391	0.2299	3.1031	0.0008	0.0001
14	0.1487	16.231	0.0015	68.68	0.1747	0.3281	1.8781	0.3129	1.7914	0.2363	0.0209
15	0.0608	1.27	0.0006	152.03	0.0647	0.1435	2.2168	0.3289	5.0809	0.0084	0.0001
16	0.1745	55.6	0.0017	35.03	0.2114	0.5605	2.6515	0.4044	1.9134	1.5872	0.0617

Table 13. All of the data about dataset 2 selected data for validation (fold 1).

Sample no	ϕ	K (mD)	ϕ (%)	FRF	ϕN	RQI	FZI	EQI	EZI	K/F	ϕHEI
1	0.1507	0.7	0.0015	34.81	0.1774	0.0676	0.3813	0.4366	2.4605	0.0201	0.0228
2	0.1049	1.967	0.0010	72.79	0.1171	0.1359	1.1602	0.3618	3.0879	0.0270	0.0021
3	0.0938	0.179	0.0009	183.55	0.1035	0.0433	0.4190	0.2410	2.3283	0.0009	0.0010
4	0.1573	17.384	0.0015	46.61	0.1866	0.3300	1.7684	0.3693	1.9785	0.3729	0.0304
5	0.0944	0.985	0.0009	90.51	0.1042	0.1014	0.9730	0.3421	3.2819	0.0108	0.0010
6	0.1544	4.093	0.0015	57.58	0.1825	0.1616	0.8854	0.3353	1.8367	0.0710	0.0268
7	0.1003	1.052	0.0010	129.18	0.1114	0.1016	0.9121	0.2778	2.4920	0.0081	0.0015
8	0.1385	16.809	0.0013	60.02	0.1607	0.3459	2.1516	0.3468	2.1574	0.2800	0.0129
9	0.1444	1.07	0.0014	51.03	0.1687	0.0854	0.5064	0.3683	2.1827	0.0209	0.0171
10	0.1279	4.678	0.0012	60.45	0.1466	0.1899	1.2948	0.3596	2.4522	0.0773	0.0076
11	0.2569	8.29	0.0025	18.58	0.3457	0.1783	0.5159	0.4577	1.3239	0.4461	0.9559
12	0.1517	1.36	0.0015	40.72	0.1788	0.0940	0.5257	0.4023	2.2499	0.0333	0.0238
13	0.074	1.72	0.0007	98.34	0.0799	0.1513	1.8943	0.3706	4.6387	0.0174	0.0002
14	0.1841	79.349	0.0018	34.56	0.2256	0.6518	2.8890	0.3964	1.7569	2.2959	0.0890
15	0.1051	0.573	0.0010	77.96	0.1174	0.0733	0.6242	0.3493	2.9746	0.0073	0.0021
16	0.208	3.78	0.0020	32.1	0.2626	0.1338	0.5096	0.3870	1.4735	0.1177	0.2086

Table 14. All of the data about dataset 2 selected data for validation (fold 2).

Sample No	ϕ	K (mD)	ϕ (%)	FRF	ϕN	RQI	FZI	EQI	EZI	K/F	ϕHEI
1	0.0755	0.061	0.0008	218.82	0.0817	0.0282	0.3456	0.2460	3.0126	0.0003	0.0003
2	0.0983	0.624	0.0010	91.92	0.1090	0.0791	0.7257	0.3327	3.0516	0.0068	0.0014
3	0.1641	5.954	0.0016	52.79	0.1963	0.1891	0.9634	0.3398	1.7307	0.1128	0.0406
4	0.1911	12.421	0.0019	41.18	0.2362	0.2531	1.0715	0.3565	1.5089	0.3016	0.1154
5	0.2091	9.827	0.0021	28.12	0.2644	0.2153	0.8142	0.4124	1.5599	0.3495	0.2166
6	0.1079	3.971	0.0011	85.16	0.1210	0.1905	1.5749	0.3299	2.7275	0.0466	0.0025
7	0.1719	1.826	0.0017	33.03	0.2076	0.1023	0.4930	0.4197	2.0217	0.0553	0.0556
8	0.1704	1.82	0.0017	33.48	0.2054	0.1026	0.4996	0.4187	2.0383	0.0544	0.0524
9	0.1995	5.7	0.0020	20.21	0.2492	0.1678	0.6735	0.4980	1.9983	0.2820	0.1557
10	0.1325	3.732	0.0013	67.64	0.1527	0.1666	1.0911	0.3340	2.1870	0.0552	0.0097
11	0.0478	2.244	0.0005	187.79	0.0502	0.2151	4.2858	0.3338	6.6489	0.0119	0.0000
12	0.192	34.2	0.0019	51.9	0.2376	0.4191	1.7636	0.3168	1.3331	0.6590	0.1192
13	0.234	3.7	0.0023	34.8	0.3055	0.1249	0.4087	0.3504	1.1471	0.1063	0.4835
14	0.186	4.64	0.0019	47.7	0.2285	0.1568	0.6863	0.3357	1.4693	0.0973	0.0956
15	0.149	5.7	0.0015	62.5	0.1751	0.1942	1.1092	0.3277	1.8716	0.0912	0.0212
16	0.171	9.3	0.0017	80.4	0.2063	0.2316	1.1226	0.2697	1.3075	0.1157	0.0537

Table 15. All of the data about dataset 2 selected data for validation (fold 3).

Sample no	ϕ	K (mD)	ϕ (%)	FRF	ϕN	RQI	FZI	EQI	EZI	K/F	ϕHEI
1	0.0755	0.061	0.0008	218.82	0.0817	0.0282	0.3456	0.2460	3.0126	0.0003	0.0003
2	0.0983	0.624	0.0010	91.92	0.1090	0.0791	0.7257	0.3327	3.0516	0.0068	0.0014
3	0.1641	5.954	0.0016	52.79	0.1963	0.1891	0.9634	0.3398	1.7307	0.1128	0.0406
4	0.1911	12.421	0.0019	41.18	0.2362	0.2531	1.0715	0.3565	1.5089	0.3016	0.1154
5	0.2091	9.827	0.0021	28.12	0.2644	0.2153	0.8142	0.4124	1.5599	0.3495	0.2166
6	0.1079	3.971	0.0011	85.16	0.1210	0.1905	1.5749	0.3299	2.7275	0.0466	0.0025
7	0.1719	1.826	0.0017	33.03	0.2076	0.1023	0.4930	0.4197	2.0217	0.0553	0.0556
8	0.1704	1.82	0.0017	33.48	0.2054	0.1026	0.4996	0.4187	2.0383	0.0544	0.0524
9	0.1995	5.7	0.0020	20.21	0.2492	0.1678	0.6735	0.4980	1.9983	0.2820	0.1557
10	0.1325	3.732	0.0013	67.64	0.1527	0.1666	1.0911	0.3340	2.1870	0.0552	0.0097
11	0.0478	2.244	0.0005	187.79	0.0502	0.2151	4.2858	0.3338	6.6489	0.0119	0.0000
12	0.192	34.2	0.0019	51.9	0.2376	0.4191	1.7636	0.3168	1.3331	0.6590	0.1192
13	0.234	3.7	0.0023	34.8	0.3055	0.1249	0.4087	0.3504	1.1471	0.1063	0.4835
14	0.186	4.64	0.0019	47.7	0.2285	0.1568	0.6863	0.3357	1.4693	0.0973	0.0956
15	0.149	5.7	0.0015	62.5	0.1751	0.1942	1.1092	0.3277	1.8716	0.0912	0.0212
16	0.171	9.3	0.0017	80.4	0.2063	0.2316	1.1226	0.2697	1.3075	0.1157	0.0537

Table 16. All of the data about dataset 2 selected data for validation (fold 4).

Sample no	ϕ	K (mD)	ϕ (%)	FRF	ϕN	RQI	FZI	EQI	EZI	K/F	ϕHEI
1	0.1312	0.404	0.1510	80.51	0.1510	0.0551	0.3649	0.3077	2.0375	0.0050	0.0091
2	0.2068	2.18	0.2607	26.27	0.2607	0.1019	0.3910	0.4290	1.6456	0.0830	0.2004
3	0.1817	1.886	0.2220	24.99	0.2220	0.1012	0.4556	0.4693	2.1135	0.0755	0.0814
4	0.138	0.75	0.1601	109	0.1601	0.0732	0.4572	0.2578	1.6106	0.0069	0.0127
5	0.133	0.42	0.1534	79.5	0.1534	0.0558	0.3637	0.3075	2.0047	0.0053	0.0099
6	0.1393	2.513	0.1618	78.89	0.1618	0.1334	0.8240	0.3017	1.8639	0.0319	0.0135
7	0.2226	11.936	0.2863	22.89	0.2863	0.2299	0.8030	0.4430	1.5472	0.5215	0.3378
8	0.1829	3.06	0.2238	33.95	0.2238	0.1284	0.5738	0.4013	1.7928	0.0901	0.0852
9	0.1245	0.472	0.1422	47.5	0.1422	0.0611	0.4299	0.4112	2.8917	0.0099	0.0064
10	0.1439	6.64	0.1681	49.14	0.1681	0.2133	1.2690	0.3761	2.2373	0.1351	0.0168
11	0.1907	13.357	0.2356	29.92	0.2356	0.2628	1.1152	0.4186	1.7767	0.4464	0.1137
12	0.102	0.938	0.1136	77.62	0.1136	0.0952	0.8383	0.3554	3.1289	0.0121	0.0018
13	0.14	4.232	0.1628	60.84	0.1628	0.1726	1.0605	0.3426	2.1048	0.0696	0.0140
14	0.1335	8.37	0.1541	76.9	0.1541	0.2486	1.6138	0.3121	2.0257	0.1088	0.0102
15	0.0643	3.07	0.0687	125.58	0.0687	0.2170	3.1573	0.3519	5.1211	0.0244	0.0001
16	0.03	0.02	0.0309	534	0.0309	0.0256	0.8290	0.2498	8.0783	0.0000	0.0000
17	0.0457	2.686	0.0479	242.75	0.0479	0.2407	5.0268	0.3002	6.2695	0.0111	0.0000

Table 17. All of the data about dataset 2 selected data for validation (fold 5).

Received: 11 April 2024; Accepted: 22 July 2024
Published online: 06 August 2024

References

1. Lim, J. S. Reservoir properties determination using fuzzy logic and neural networks from well data in offshore Korea. *J. Petrol. Sci. Eng.* **49**, 182–192 (2005).
2. Al-Jawad, S. N. & Saleh, A. H. Flow units and rock type for reservoir characterization in carbonate reservoir: Case study, south of Iraq. *J. Petrol. Explor. Prod. Technol.* **10**, 1–20 (2020).
3. Kargarpour, M. A. Carbonate reservoir characterization: An integrated approach. *J. Petrol. Explor. Prod. Technol.* **10**, 2655–2667 (2020).
4. Malki, M. L. *et al.* Underlying mechanisms and controlling factors of carbonate reservoir characterization from rock physics perspective: A comprehensive review. *Geoenergy Sci. Eng.* **226**, 211793 (2023).
5. Jamshidi Gohari, M. S., Emami Niri, M., Sadeghnejad, S. & Ghiasi-Freez, J. Synthetic graphic well log generation using an enhanced deep learning workflow: Imbalanced multiclass data, sample size, and scalability challenges. *SPE J.* **29**, 1–20 (2023).
6. Bakhshian, S., Rabbani, H. S., Hosseini, S. A. & Shokri, N. New insights into complex interactions between heterogeneity and wettability influencing two-phase flow in porous media. *Adv. Earth Space Sci.* **47**, 88187 (2020).
7. Li, W. *et al.* Pore-throat structure characteristics and its impact on the porosity and permeability relationship of Carboniferous carbonate reservoirs in eastern edge of Pre-Caspian Basin. *Pet. Explor. Dev.* **47**, 1027–1041 (2020).
8. Mohammadi, M., Shadizadeh, S. R., Khaksar Manshad, A. & Mohammadi, A. H. Experimental study of the relationship between porosity and surface area of carbonate reservoir rocks. *J. Petrol. Sci. Eng.* **10**, 1817–1834 (2020).
9. Khosravi, M. H., Emami Niri, M. & Saberi, M. R. Effects of diagenetic processes on the velocity evolution in carbonate reservoirs. *Geomech. Geophys. Geo-Energy Geo-Resour.* **9**, 147 (2023).
10. Chilingarian, G. V., Mazzullo, S. J. & Rieke, H. H. *Carbonate Reservoir Characterization: A Geologic-Engineering Analysis* Vol. 1 (Elsevier Science, 1992).
11. Babadagli, T. & Al-Salmi, S. A review of permeability-prediction methods for carbonate reservoirs using well-log data. *SPE Reserv. Eval. Eng.* **7**, 75–88 (2004).
12. Tavakoli, V. Carbonate reservoir heterogeneity overcoming the challenges. In *Springer Brief in Petroleum Geoscience & Engineering* (ed. Tavakoli, V.) (Springer International Publishing, 2019).
13. Emami Niri, M., Mehmandoost, F. & Nosrati, H. Pore-type identification of a heterogenous carbonate reservoir using rock physics principles: A case study from south-west Iran. *Appl. Geophys.* **69**, 1241–1256 (2021).
14. Stadtmuller, M. & Jarzyna, J. A. Estimation of petrophysical parameters of carbonates based on well logs and laboratory measurements, a review. *Energies* **16**, 4215 (2023).
15. Alhammadi, A. M., Gao, Y., Akai, T., Blunt, M. J. & Bijeljic, B. Pore-scale x-ray imaging with measurement of relative permeability, capillary pressure and oil recovery in a mixed-wet micro-porous carbonate reservoir rock. *Fuel* **268**, 117018 (2020).
16. Faramarzi-Palangar, M., Mirzaei-Paiaman, A., Ghoreishi, S. A. & Ghanbarian, B. Wettability of carbonate reservoir rocks: A comparative analysis. *Appl. Sci.* **12**, 131 (2021).
17. Rashid, F., Hussein, D., Lorinczi, P. & Glover, P. W. J. The effect of fracturing on permeability in carbonate reservoir rocks. *Mar. Petrol. Geol.* **152**, 106240 (2023).
18. Khairi, H. & Harith, Z. Z. T. Influence of pore geometry, pressure and partial water saturation to electrical properties of reservoir rock: Measurement and model development. *J. Petrol. Sci. Eng.* **78**, 687–704 (2011).
19. Norbisrath, J. H., Weger, R. J. & Eberli, G. P. Complex resistivity spectra and pore geometry for predictions of reservoir properties in carbonate rocks. *J. Petrol. Sci. Eng.* **151**, 455–467 (2017).
20. Regnet, J. B., David, C., Robion, P. & Menendez, B. Microstructures and physical properties in carbonate rocks: A comprehensive review. *Mar. Petrol. Geol.* **103**, 366–376 (2019).
21. Tariq, Z., Mahmoud, M., Al-Youssef, H. & Khan, M. R. Carbonate rocks resistivity determination using dual and triple porosity conductivity models. *Petroleum* **6**, 35–42 (2020).
22. Soleymanzadeh, A., Helalizadeh, A., Jamialahmadi, M. & Soltani Soulgani, B. Development of a new model for prediction of cementation factor in tight gas sandstones based on electrical rock typing. *J. Nat. Gas Sci. Eng.* **94**, 104128 (2021).

23. Kolah-Kaj, P., Kord, S. H. & Soleymanzadeh, A. The effect of pressure on electrical rock typing, formation resistivity factor, and cementation factor. *J. Petrol. Sci. Eng.* **204**, 108757 (2021).
24. Soleymanzadeh, A., Parvin, S. & Kord, S. H. Effect of overburden pressure on determination of reservoir rock types using RQI/FZI, FZI* and Winland methods in carbonate rocks. *Petrol. Sci.* **16**, 1403–1416 (2019).
25. Baraboshkin, E. E. *et al.* Deep convolutions for in-depth automated rock typing. *Comput. Geosci.* **135**, 104330 (2020).
26. Najafi-Silab, R., Soleymanzadeh, A., Kolah-Kaj, P. & Kord, S. H. Electrical rock typing using Gaussian mixture model to determine cementation factor. *J. Petrol. Explor. Prod. Technol.* **13**, 1–16 (2023).
27. Aman e Room, Sh., Zhonghong, Ch., Ullah, H., Ahmad, W. & Ali, M. Reservoir characteristics and controlling factors of Permian glutenite in Northern Zhongghai uplift, Junggar Basin, China. *Ore Energy Resour. Geol.* **15**, 100025 (2023).
28. McKinley, J. M., Atkinson, P. M., Lloyd, C. D., Ruffell, A. H. & Worden, R. H. How porosity and permeability vary spatially with grain size, sorting, cement volume, and mineral dissolution in fluvial Triassic sandstones: The value of geostatistics and local regression. *J. Sediment. Res.* **81**, 844–858 (2011).
29. Wang, J., Ye, F., Zhang, Ch. & Xi, Zh. Factors that control the reservoir quality of the Carboniferous-Permian tight sandstones in the Shilounan block, Ordos basin. *Processes* **11**, 2279 (2023).
30. Soleymanzadeh, A., Jamialahmadi, M., Helalizadeh, A. & Soltani Soulgani, B. A new technique for electrical rock typing and estimation of cementation factor in carbonate rocks. *J. Petrol. Sci. Eng.* **166**, 381–388 (2018).
31. Klyuchnikov, N. *et al.* Data-driven model for the identification of the rock type at a drilling bit. *J. Petrol. Sci. Eng.* **178**, 506–516 (2019).
32. Mohammadian, E., Kheirollahi, M., Liu, B., Ostadhassan, M. & Sabet, M. A case study of petrophysical rock typing and permeability prediction using machine learning in a heterogenous carbonate reservoir in Iran. *Sci. Rep.* **12**, 4505 (2023).
33. Radwan, A. E., Wood, D. A. & Radwan, A. A. Machine learning and data-driven prediction of pore pressure from geophysical logs: A case study for the Mangahewa gas field, New Zealand. *J. Rock Mech. Geotech. Eng.* **14**, 1799–1809 (2022).
34. Sanguino, A., Lenim, C. Petrophysical rock typing in Uinta basin using models powered by machine learning algorithms. Master of Science Degree, Norman, Oklahoma (2023).
35. Anselmetti, F. S., Luthi, S. & Eberli, G. P. Quantitative characterization of carbonate pore systems by digital image analysis. *Am. Assoc. Petrol. Geol.* **82**, 1815–1836 (1998).
36. Garing, C. *et al.* Electrical and flow properties of highly heterogeneous carbonate rocks. *Am. Assoc. Petrol. Geol. Bull.* **98**, 49–66 (2013).
37. Norbisrath, J. H. *et al.* Electrical and fluid flow properties of carbonate microporosity types from multiscale digital image analysis and mercury injection. *Am. Assoc. Petrol. Geol. Bull.* **99**, 2077–2098 (2015).
38. Zhang, Z., Cai, Z., Zhang, H. & Li, J. Comparative study on hydraulic and electrical transport properties of carbonate rocks based on rock typing. *J. Energy Fuels* **37**, 2759–2773 (2023).
39. Aftab, S., Leisi, A. & Kadkhodaie, A. Reservoir petrophysical index (RPI) as a robust tool for reservoir quality assessment. *Earth Sci. Inform.* **16**, 2457–2473 (2023).
40. Hou, Y. *et al.* Numerical simulation of electrical properties of carbonate reservoirs using digital rocks. *Processes* **11**, 2214 (2023).
41. Nourani, M. *et al.* Analytical models for predicting the formation resistivity factor and resistivity index at overburden conditions. *Petrophysics* **64**, 353–366 (2023).
42. Rezaei, A. *et al.* Insights into the effects of pore size distribution on the flowing behavior of carbonate rocks: Linking a nano-based enhanced oil recovery method to rock typing. *MDPI* **10**, 972 (2020).
43. Soleymanzadeh, A., Kolah-Kaj, P., Kord, Sh. & Monjezi, M. A new technique for determining water saturation based on conventional logs using dynamic electrical rock typing. *J. Nat. Gas Sci. Eng.* **196**, 107803 (2021).
44. Archie, G. E. The electrical resistivity log as an aid in determining some reservoir characteristics. *Trans. AIME* **146**, 54–62 (1942).
45. Attia, A. M. Effects of petrophysical rock properties on tortuosity factor. *J. Petrol. Sci. Eng.* **48**, 185–198 (2005).
46. Kolah-Kaj, P., Kord, S. H. & Soleymanzadeh, A. Application of electrical rock typing for quantification of pore network geometry and cementation factor assessment. *J. Petrol. Sci. Eng.* **208**, 109426 (2022).
47. Rezaei, H., Dehghan Monfared, A. & Soleymanzadeh, A. Cementation factor in clayey rock samples: investigation the role of clay content and determination using electrical rock classification. *Appl. Clay Sci.* **234**, 106849 (2023).
48. Hassanzadeh, A. J., Javaherian, A., Pishvaie, M. R. & Nabi-Bidhendi, M. An approach to defining tortuosity and cementation factor in carbonate reservoir rocks. *J. Petrol. Sci. Eng.* **60**, 125–131 (2008).
49. Byun, Y. H., Hong, W. T. & Yoon, H. K. Characterization of cementation factor of unconsolidated granular materials through time domain reflectometry with variable saturated conditions. *Materials* **12**, 1340 (2019).
50. Akpabio, I., Atat, J., Umoren, E. & Ekemini, J. D. The reservoir rock volumetric concentration and tortuosity description of pore space of Xa field, Niger Delta basin. *World J. Adv. Sci. Technol.* **3**, 1–13 (2023).
51. Rezaee, M. R., Motiei, H. & Kazemzadeh, E. A new method to acquire m exponent and tortuosity factor for microscopically heterogeneous carbonates. *J. Petrol. Sci. Eng.* **56**, 241–251 (2007).
52. Mohammadi, M. *et al.* A novel electrical rock typing approach to improve estimating formation resistivity factor in carbonate rocks. *NIOC Exploration Directorate* (2020).
53. Rushing, J. A., Newsham, K. E., Blasingam, T. A. Rock typing—Keys to understanding productivity in tight gas sands. *In SPE Unconventional Reservoirs Conference Keystone, Colorado* (2008).
54. Mirzaei-Paiaman, A., Ostadhassan, M., Rezaee, R., Saboorian-Jooybari, H. & Chen, Z. H. A new approach in petrophysical rock typing. *J. Petrol. Sci. Eng.* **166**, 445–464 (2018).
55. Prakoso, S., Irham, S., Herdiansyah, F., Burhannudinnur, M., Putra, R. A., Khairy, H., Irano, T. Rock type, diagenesis, and sonic velocity to understanding carbonate reservoirs: A case study in TKA oil field. In *AIP Conference Proceedings*, 2598 (2023).
56. Onuh, H. M., David, O. O. & Onuh, Ch. Y. Modified reservoir quality indicator methodology for improved hydraulic flow unit characterization using the normalized pore throat methodology (Niger Delta field as case study). *J. Petrol. Explor. Prod. Technol.* **7**, 409–416 (2017).
57. Thota, S. T., Islam, M. A. & Shalaby, M. R. Reservoir quality evaluation using sedimentological and petrophysical characterization of deep-water turbidites: A case study of Tariki sandstone member, Taranaki basin, New Zealand. *Energy Geosci.* **4**, 13–32 (2023).
58. Nwokoma, E. U., Ijeh, B. I. & Amos-Uhegbu, Ch. Hydraulic flow unit characterization in sandstone reservoirs, Niger Delta, Nigeria. *Earth Planet. Sci.* **2**, 1–10 (2023).
59. Abraham-A, R. M., Tassinari, C. C. C. G., Taioli, F., Rocha, H. V. & Silva, O. C. D. Reservoir quality evaluation as a measure to forecast hydrocarbon and CO2 storage prospects in Irati and Rio Bonito formations, Parana basin. *Results Geophys. Sci.* **14**, 100059 (2023).
60. Amaefule, J. O. et al. Enhanced reservoir description: using core and log data to identify hydraulic (flow) units and predict permeability in uncored intervals/wells. In *SPE Annual Technical Conference and Exhibition*, 205–220 (1993).
61. Boualam, A. & Djezzar, S. Integration of rock types and hydraulic flow units for reservoir characterization. Application to three forks formation, Williston basin, North Dakota, USA. *WILEY Online Libr.* **17**, 147–162 (2023).
62. Krivoshchekov, S. *et al.* Rock typing approaches for effective complex carbonate reservoir characterization. *Energies* **16**, 6559 (2023).
63. Xu, Ch. *et al.* Connate water saturation—Irreducible or not: The key to reliable hydraulic rock typing in reservoirs straddling multiple capillary windows. *SPE J.* https://doi.org/10.2118/166082-MS (2013).

64. Liu, Y. *et al.* Petrophysical static rock typing for carbonate reservoirs based on mercury injection capillary pressure curves using principal component analysis. *J. Petrol. Sci. Eng.* **181**, 106175 (2019).
65. Sawayama, K. *et al.* Relating hydraulic-electrical-elastic properties of natural rock fractures at elevated stress and associated transient changes of fracture flow. *Rock Mech. Rock Eng.* **54**, 2145–2164 (2021).
66. El-Sayed, A. M. *et al.* Rock typing based on hydraulic and electric flow units for reservoir characterization of Nubia sandstone, south-west Sinai, Egypt. *J. Petrol. Explor. Prod. Technol.* **11**, 3225–3237 (2021).
67. Barach, B. A. B. et al. Development and Identification of Petrophysical Rock Typing for Effective Reservoir Characterization. In *SPE Nigeria Annual International Conference and Exhibition, Lagos, Nigeria, August* (2022).
68. Tong, X., Yan, L. & Xiang, K. A prediction method of compacted rock hydraulic permeability based on the MGEMTIP model. *Minerals* **13**, 281 (2023).
69. Ragland, D. A. Trends in cementation exponents (m) for carbonate pore systems. *SPWLA J. Form. Eval. Reserv. Descr.* **43**, 434–446 (2002).
70. Laursen, G. V. et al. The Asmari formation revisited: Changed stratigraphic allocation and new biozonation. In *EAGE International Petroleum Conference and Exhibition* (2009).
71. Mohammadi, Z., Mehrabi, H., Gharechelou, S., Jalali, M. & Swennen, R. Stratigraphic architecture and depositional diagenetic evolution of Oligocene-Miocene carbonate-evaporate platform in the southern margin of the Neo-Tethys Ocean, Lurestan zone of Zagros, Iran. *J. Asian Earth Sci.* **233**, 105249 (2022).
72. Abdolahi, A., Bahrevar, M., Chehrazi, A., Kadkhodaie, A. & Wood, D. A. Integration of geoscience data to delineate quality of the Asmari reservoir, Iranian part of the Persian Gulf basin. *Mar. Petrol. Geol.* **152**, 106229 (2023).
73. Adams, T. D., Bourgeios, F. Asmari biostoatigraphy, geological and exploration. *Div, Jooc Report*, 1074 (1967).

Author contributions

Milad Mohammadi: Investigation, Visualization, Writing-Original Draft, Conceptualization, Validation, Modeling, Mohammad Emami Niri: Writing-Review & Editing, Methodology, Validation, Supervision, Data curation, Abbas Bahroudi: Writing-Review & Editing, Validation, Supervision, Data curation, Shahin Kord: Writing-Review & Editing, Validation, Aboozar Soleymanzadeh: Writing-Review & Editing, Validation, Methodology.

Competing interests

The authors declare no competing interests.

Additional information

Correspondence and requests for materials should be addressed to M.E.N.

Reprints and permissions information is available at www.nature.com/reprints.

Publisher's note Springer Nature remains neutral with regard to jurisdictional claims in published maps and institutional affiliations.